



HAL
open science

Stratigraphic architecture of a saline lake system: From lake depocentre (Alès Basin) to margins (Saint-Chaptes and Issirac basins), Eocene–Oligocene transition, south-east France

Alexandre Lettéron, Youri Hamon, François Fournier, François Demory, Michel Séranne, Philippe Joseph

► To cite this version:

Alexandre Lettéron, Youri Hamon, François Fournier, François Demory, Michel Séranne, et al.. Stratigraphic architecture of a saline lake system: From lake depocentre (Alès Basin) to margins (Saint-Chaptes and Issirac basins), Eocene–Oligocene transition, south-east France. *Sedimentology*, 2022, 69 (2), pp.651-695. 10.1111/sed.12920 . hal-03406458

HAL Id: hal-03406458

<https://hal.science/hal-03406458>

Submitted on 14 Mar 2022

HAL is a multi-disciplinary open access archive for the deposit and dissemination of scientific research documents, whether they are published or not. The documents may come from teaching and research institutions in France or abroad, or from public or private research centers.

L'archive ouverte pluridisciplinaire **HAL**, est destinée au dépôt et à la diffusion de documents scientifiques de niveau recherche, publiés ou non, émanant des établissements d'enseignement et de recherche français ou étrangers, des laboratoires publics ou privés.

Stratigraphic architecture of a saline lake system: From lake depocentre (Alès Basin) to margins (Saint-Chaptes and Issirac basins), Eocene-Oligocene transition, south-east France.

Alexandre Lettéron ^{a,b*}, Youri Hamon ^a, François Fournier ^b, François Demory ^b, Michel Séranne ^c,
Philippe Joseph ^a.

a – IFP Energies nouvelles (IFPEN), 1-4, avenue de Bois-Préau, 92852 Rueil-Malmaison, France.

b – Aix Marseille Univ, CNRS, IRD, INRAE, Coll France, CEREGE, Aix-en-Provence, France

c – Geosciences Montpellier, Université de Montpellier, 34095 Montpellier Cedex 05, France.

*Alexandre Lettéron: alexandre.letteron@gmail.com

Sedimentology Journal - <https://doi.org/10.1111/sed.12920> – First Published: 14 July 2021

ABSTRACT

Changes in sedimentary profiles and stratigraphic architecture over time in lake basins are shown to be relevant markers of climate changes in terrestrial palaeoenvironments. The stratigraphic architecture of the Priabonian (late Eocene)-early Rupelian (early Oligocene) Alès-Saint-Chaptes-Issirac saline lake system has been reconstructed from the sedimentological, biostratigraphic and magnetostratigraphic analysis of outcrops and well cores. As a function of the inflow-evaporation balance, three distinct depositional models have been proposed for the Priabonian Alès-Saint-Chaptes-Issirac lake system which is characterized by both fault-controlled and low-angle ramp-like margins: (i) freshwater to oligohaline lake; (ii) oligohaline to mesohaline closed-lake; and (iii) hypersaline, evaporitic closed-lake. Two major stages of lake spreading (middle Priabonian and late Priabonian-early Rupelian?) separated by two stages of significant lake closure represented by evaporite succession in the Alès Basin depocentre (middle to late Priabonian) have been evidenced. Regional tectonics and climate induced changes in inflow-evaporation balance of the lake and controlled the development of transgressive-regressive cycles with calcium-sulphate sedimentation during regression in the lake depocentre (Alès Basin) and during early transgression in lake margins (Saint-Chaptes and Issirac basins). The correlation between the palaeohydrological cycles inferred for the Alès-Saint-Chaptes-Issirac lake system and the regional climate changes of Priabonian stage, prior to the Eocene-Oligocene transition, strongly suggests that climate significantly impacted the nature of lacustrine depositional models and the depositional architecture of Palaeogene, syn-rift, saline lake basins from Western Europe.

Keywords: *Calcium sulphates, depositional models, lacustrine carbonates, palaeoclimate, Priabonian, salt lakes, stratigraphic architecture.*

INTRODUCTION

Extensive saline lake environments developed in the basins of the European Cenozoic Rift System (ECRIS) during Priabonian (late Eocene) and Rupelian (early Oligocene) stages (Ziegler, 1992; Rouchy, 1997) (Fig. 1). They are characterized by the deposition of thick carbonate and calcium sulphate successions (e.g. Rouchy, 1997). The deepest and most subsiding segments of such rift basins (Upper Rhine Graben, Bresse, Valence and Camargue Basins) are characterized by confined conditions favouring chloride and potash salt precipitation (e.g. Dumas, 1987; Blanc-Valleron, 1991; Curial & Moretto, 1997). Coeval development of lacustrine carbonates associated with the deposition of calcium sulphates occurred in the Alès, Saint-Chaptes and Issirac basins (referred to the ASCI lake system) (Busson *et al.*, 1992; Lettéron *et al.*, 2017, 2018) as well as in the Mormoiron-Carpentras and Apt-Manosque-Forcalquier basins (e.g. Triat & Truc, 1972; Cavelier, 1984) (Fig. 1).

The oil exploration surveys conducted since the 1940s in the south-eastern rift basins of France, and most particularly in the Alès Basin (Fig. 2; Table 1), led to the acquisition of a comprehensive subsurface database (cores, well-logs, two-dimensional seismic). Such a database represents a unique archive that offers great opportunities to link the syn-rift basin-fill architecture and the evolution of the ASCI saline lake during a period of major global and regional climatic changes affecting both marine and continental domains (e.g. Liu *et al.*, 2009; Pound & Salzmann, 2017; Tanrattana *et al.*, 2020). This climate change recorded close to the Eocene-Oligocene transition (EOT, ca 33-34 Ma) was revealed by an abrupt shift in $\delta^{18}\text{O}$ values of deep-marine carbonates reflecting the first glaciation of Antarctica and the cooling of the surface and deep oceanic waters (e.g. Zachos *et al.*, 2001). In addition, a major faunal turnover across Europe known as 'The Grande Coupure' occurred (e.g. Costa *et al.*, 2011). In past studies, considerable attention has been paid to the structural and kinematic evolution of the Alès Basin (Roure *et al.*, 1992; Séranne *et al.*, 1995; Benedicto-Esteban, 1996; Sanchis & Séranne,

2000), but no result has been published regarding the nature and the evolution of the syn-rift sedimentation at the ASCI lake system depocentre which is accessible only through subsurface data.

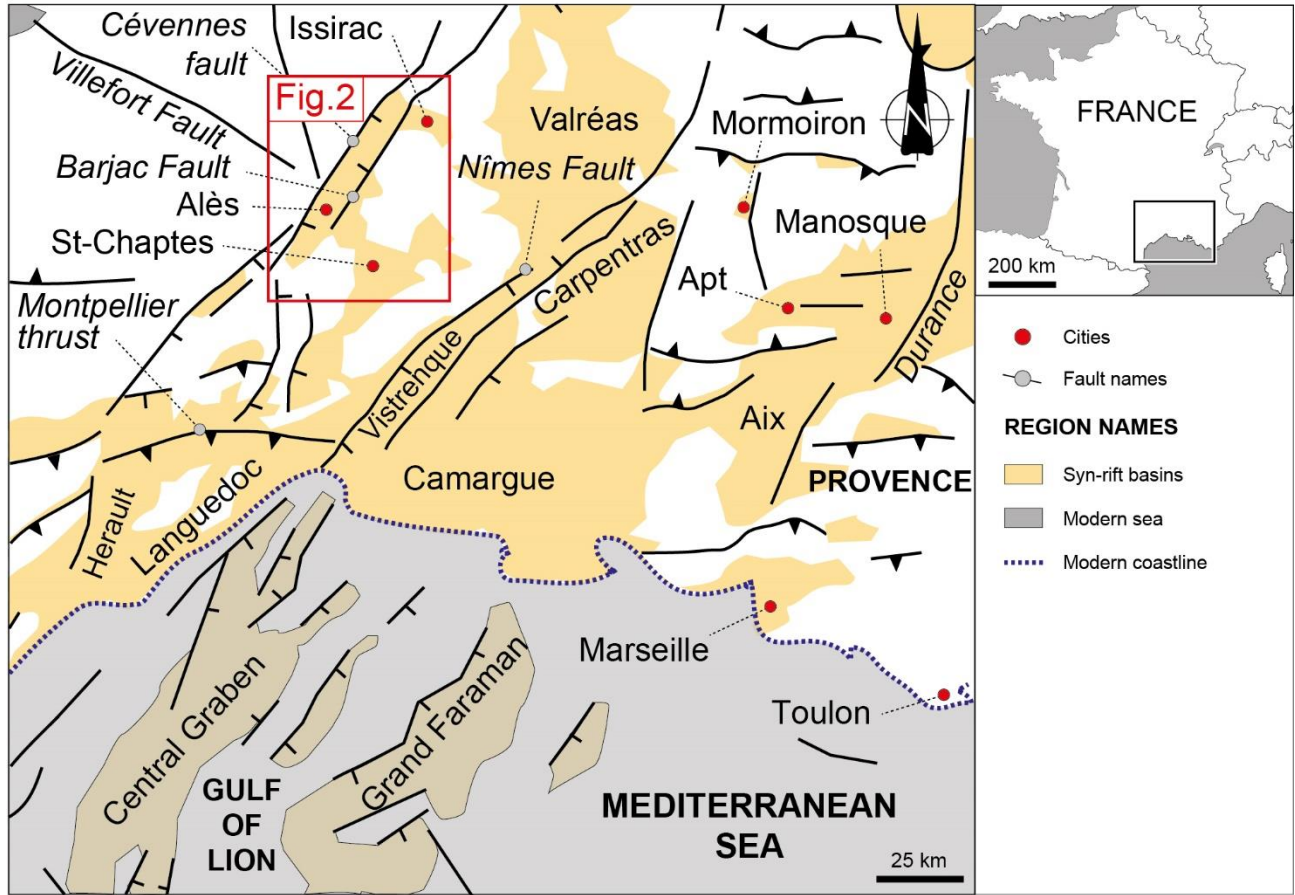


Fig. 1. Location map of the study area. Simplified map of the southern France highlighting the main Cenozoic sedimentary basins, major faults and regions, modified after Andeweg (2002).

In contrast, marginal lake deposits are widely exposed in the adjacent Issirac and Saint-Chaptes basins as two lacustrine gulfs and to a lesser extent in the eastern margin of the Alès Basin (Alabouvette *et al.*, 1983; Chedhomme & Gaudant, 1984; Frédet, 1987) which made it possible to provide detailed lithofacies classifications and to reconstruct depositional profiles for shallow, saline-water, lacustrine and palustrine environments (Lettéron *et al.*, 2017, 2018).

In addition to sequence stratigraphic analysis, the interactions between structural and climatic controls on depositional profiles and stratigraphic architecture in lacustrine rift basins are gaining

increasing attention (Bergner *et al.*, 2009; Nutz *et al.*, 2017, 2019; Newell, 2018; Zhang *et al.*, 2018, 2020; Rohais *et al.*, 2019; Favoreto *et al.*, 2021). However, various knowledge gaps still exist regarding the relative impact of climate and tectonics on lacustrine depositional models and on the development of transgressive–regressive cycles in saline lakes from ancient and modern rift and post-rift basins (e.g. Harris *et al.*, 2012; Wright, 2012; Varejão *et al.*, 2019).

The detailed sedimentological analysis of both outcrops and subsurface data from the syn-rift Priabonian ASCI lake system provides an excellent opportunity to relate the sedimentary architecture and the evolution through time of depositional profiles during the Priabonian which is a period of terrestrial climatic transition which preceded the major EOT event (Pound & Salzmann, 2017). In the present work a special focus will be given to the underexplored stratigraphic relationships between lake margins and lake basin depocentre in saline lacustrine rift basins, which implies the definition of a well-constrained chronostratigraphic framework.

Based on the petrographical and sedimentological analyses of Alès Basin well cores, the acquisition of magnetostratigraphic data from the Priabonian–early Rupelian (?) field section in the Issirac Basin, and the integration of all previously published biostratigraphic markers and sedimentological analyses from the ASCI lake system (Lettéron *et al.*, 2017, 2018, and references therein), the present work aims to: (i) establishing a chronostratigraphic framework of the Priabonian ASCI lake deposits; (ii) proposing depositional models for the ASCI saline lake at various stages of the Priabonian palaeoclimatic evolution; and (iii) discussing the temporal and spatial relationships between lake margins and lake depocentre areas.

These results will have significant implications for the definition of the timing and modalities of climate changes in Western Europe during the Priabonian and will serve to highlight the impact of climate on the development and the nature of depositional sequences in lake basins.

GEOLOGICAL SETTING

The Priabonian ASCI lake occupies a relatively narrow (ca 55 x 6 km) north-east/south-west elongated basin (Alès Basin) and two subsidiary basins (Figs 2 and 3A): the Issirac Basin (ca 15 x 5 km) to the north-east and the Saint-Chaptes Basin (ca 25 x 10 km) to the south-east. The Alès Basin formation was initiated during the European Cenozoic Rifting phase (Priabonian-Rupelian) and then reactivated during the Liguro-Provençal Rifting phase (Chattian-Aquitainian) (Séranne *et al.*, 1995). Such a polyphased tectonic setting led to a composite structural style (Benedicto-Esteban, 1996) (Fig. 3B). During the late Eocene, the half-graben geometry of the Alès Basin and the associated hangingwall roll-over were controlled by the N10°-N30° Alès listric fault (Sanchis & Séranne, 2000) (Fig. 3A and B). The interpretation of two-dimensional seismic profiles provided evidence that thin-skinned deformation was responsible for the propagation of the Alès listric fault as a complex extensional ramp-flat system and for the formation of a hangingwall syncline basin during the late Priabonian to Rupelian (Sanchis & Séranne, 2000) (Fig. 3B). Finally, the Priabonian Alès and Saint-Chaptes basins have been shown to form as a result of a left-lateral shearing of the area comprised between the north-east-trending Cévennes and Nîmes faults (Séranne *et al.*, 2021). Such a left-lateral strike-slip along north-east-trending faults accommodates east-west extension of the West European Rift (ECRIS) and part of the ongoing north-south shortening in the Central and Western Pyrénées. In the Saint-Chaptes (Lettéron *et al.*, 2018) and Issirac basins (Lettéron *et al.*, 2017), the palustrine to the Saint-Chaptes (Lettéron *et al.*, 2018) and Issirac basins (Lettéron *et al.*, 2017), the palustrine to shallow lacustrine deposits (Lettéron *et al.*, 2017, 2018) overlie N110° trending pre-rift syncline structures inherited from the main phase of the Pyrenean orogeny (Late Cretaceous-Eocene compressional event) (Sanchis & Séranne, 2000) (Fig. 3A). This multiphase tectonic history and the resulting structural configuration enhanced the development of narrow palaeolake margins in the Alès Basin bordered

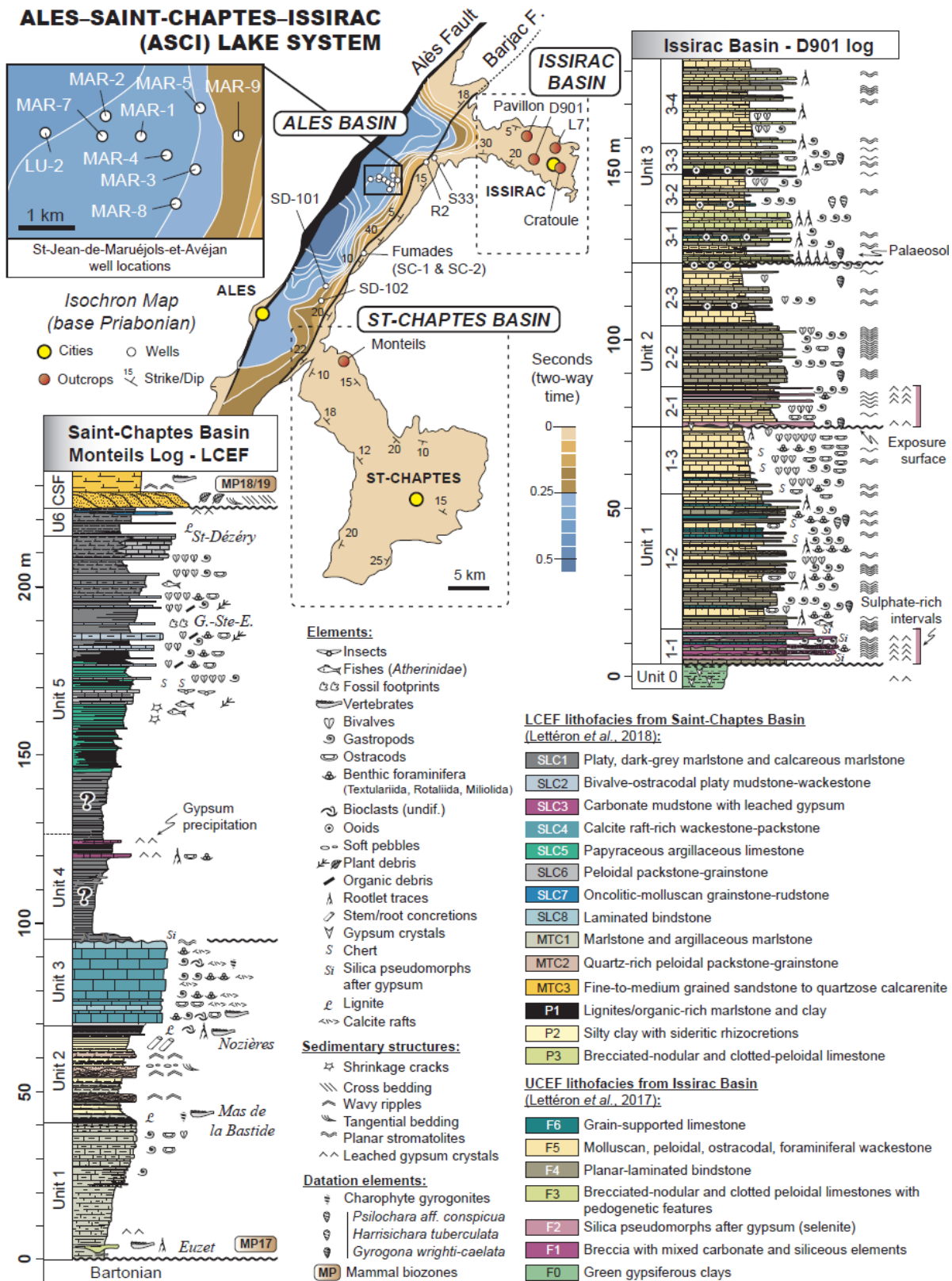


Fig. 2. Isochron map of the base Priabonian with outcrop and well locations, modified after Benedicto-Esteban (1996). Detailed stratigraphy of Issirac Basin [D901 log modified after Lettéron et al. (2017)] and Saint-Chaptes Basin [Monteils log modified after Lettéron et al. (2018)]. LCEF - Lower Carbonate and Evaporite Formation, CSF - Célas Sandstone Formation; UCEF - Upper Carbonate and Evaporite Formation; sensu Lettéron et al. (2018).

by faults, except at the intersection with the Saint-Chaptes and Issirac syncline basins which promote the development of extensive shallow lake areas (Fig. 3A). Palaeotopographic configuration controlled by extensive faults and folding favoured higher subsidence rates in the Alès Basin (lake system depocentre) than the Issirac and Saint-Chaptes adjacent syncline basins (lake system margins) (Fig. 2). The depocentre of the ASCI lake system is located close to the Alès listric fault in the Alès Basin as illustrated by the isochron map of the base Priabonian seismic marker (Fig. 2).

The ASCI lake system developed coevally with other rift basins in the Rhodanian area, such as the Mormoiron–Carpentras, Apt–Manosque–Forcalquier basins and possibly the Camargue graben, where saline lacustrine carbonate and evaporite deposits have been documented (e.g. Rouchy, 1997). The Priabonian salt lake basins from the ECRIS developed during a major transitional climatic period (Soták, 2010) that preceded the Eocene–Oligocene transition. The origin of solutes in lacustrine environments of the ECRIS basins has been discussed extensively over the last decades: recycling of Triassic evaporites from surface leaching or groundwater circulations is considered a possible source of calcium sulphate in the ECRIS lake basins (e.g. Truc, 1978; Fontes *et al.*, 1996), but some sporadic marine connections may also have fed the lake systems with saline waters (e.g. Moretto, 1988).

Numerous fossil sites discovered in the study area provided various mammal (Rémy, 1994, 1999, 2015) and charophyte (Feist-Castel, 1971; Lettéron *et al.*, 2017) biostratigraphic constraints (see Monteils and D901 logs - Fig. 2). The Saint-Hippolyte-de-Caton fauna or also known as Euzet-les-Bains fauna of the Unit 1 (*sensu* Lettéron *et al.*, 2018) defined in the Saint-Chaptes Basin were dated by Remy (1999) to the early Priabonian (MP17A mammal zone). The Célas Sandstone Formation (CSF) fauna includes crocodylians, marsupials, rodents, turtles, squamates, perissodactyls and artiodactyles. Garimond & Thaler (1963) assigned a MP19 mammal age but the latest research of Remy (1985, 1999) assigned an age between La Débruge (MP18) and Montmartre (MP19) Priabonian mammal zones. Grambast (1962), Feist-Castel (1971) and Lettéron *et al.* (2018) recognized among the charophytes

collected in the ASCI lake system, charophyte gyrogonites dated from the early Priabonian [*Psilochara repanda* charophytes zones of Riveline *et al.* (1996)] to the late Priabonian (*Stephanochara vectensis*). No magnetostratigraphic interpretations are available and strontium isotope ratios of carbonates coincide with Priabonian–Rupelian marine values but also with those of Triassic evaporites (Lettéron *et al.*, 2018).

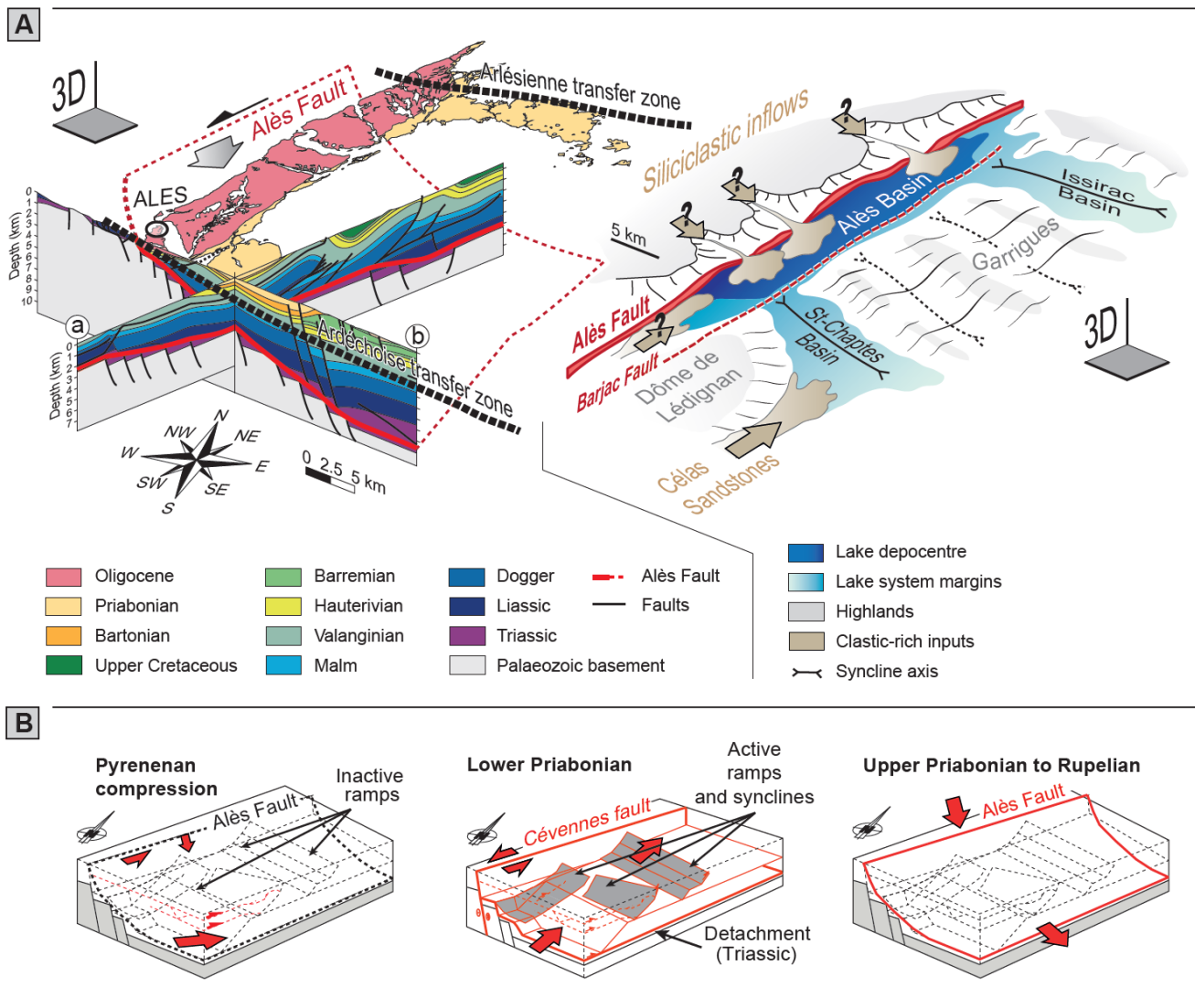


Fig. 3. Alès, Saint-Chaptes and Issirac (ASCI) lake system geological settings: (A) structure and palaeogeographic domains of the ASCI lake system, modified after Lettéron *et al.* (2018); (B) tectonic evolution of the Alès Basin, modified after Sanchis (2000).

DATABASE AND METHODS

The present work is based on subsurface data (cores and well-logs) from 11 wells located in the Alès Basin (Table 1) as well as magnetostratigraphic data from the Issirac Basin. It also integrates the published palaeontological and sedimentological dataset from Issirac (Lettéron *et al.*, 2017) and Saint-Chaptes basins (Lettéron *et al.*, 2018) (see locations on Fig. 2).

Table 1. List of subsurface database.

Well ID	Locations	Well logs and mud logging report (MLR)	Studied core intervals	Max Depth	Completion
LU-2	Saint-Victor-de-Malcap	Well logs (SP, Res) + MLR	-	1993 m	1951-1952
MAR-1	Saint-Victor-de-Malcap	Well logs (GR, SP, Res) + MLR	Cuttings from 400-1330 m	1566 m	1947-1948
MAR-3	Rochegude	Well logs (SP, Res) + MLR	-	888 m	1949
MAR-4	Rochegude	Well logs (SP, Res) + MLR	-	1788 m	1949-1950
MAR-7	Saint-Victor-de-Malcap	Well logs (SP, Res) + MLR	-	930 m	1949-1950
MAR-101	Saint-Victor-de-Malcap	Well logs (DT, SPHI, GR) + MLR	Cores from 744-872 m	917 m	1980
SD-101	Salindres	Well logs (SP, Res) + MLR	Cores from 230-650 m	1648.8 m	1961-1962
SC-1	Allègres-les-Fumades	-	Cores from 0-120 m	122 m	2007
SC-2	Allègres-les-Fumades	-	Cores from 0-120 m	122 m	2007

Petrographic and core analysis

Petrographic analyses are based on macroscopic observations of well cores and outcrop rock samples from the Alès Basin, as well as on the study of 265 thin sections under polarized-light microscopy. The subsurface dataset is mainly inherited from the oil and gas exploration conducted in the 1940s in south-east France. Cores and side-wall samples from three exploration wells located in the Alès Basin were analyzed: MAR-1 (Fig. 4A) and its equivalent well core interval MAR-101 (St-Jean-de-Maruejols-et-Avéjan) (Fig. 4B and C) and SD-101 (Salindres) (Fig. 4D) (see well locations on Fig. 2). In addition, the present subsurface dataset integrates two *ca* 106 m cores (SC-1 and SC-2), recovered in 2007 for the assessment of water resources of the Allègre-les-Fumades thermal springs (Fig. 4E). The stratigraphic gap between SC-1 and SC-2 cored intervals has been estimated to average 45 m, according to the distance between the two wells (*ca* 370 m), the strike and dip of regional geology

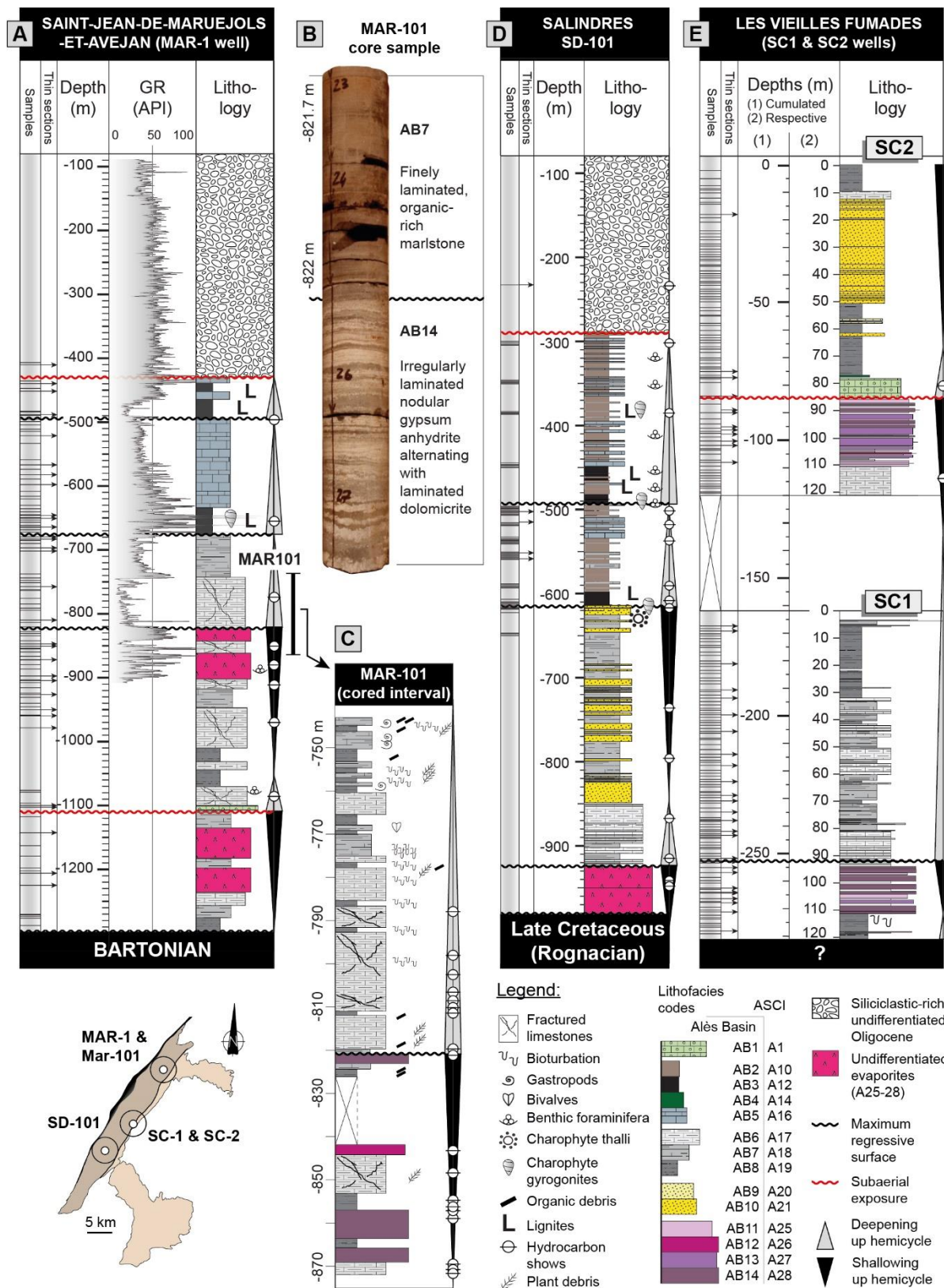


Fig. 4. Lithology and depositional lithofacies of Priabonian deposits from Alès Basin wells: (A) Saint-Jean-de-Maruéjols-et-Avéjan 1 - MAR-1; (B) MAR-101 core sample photography (from -822.4 to -821.7 m); (C) MAR-1 cored interval (MAR-101) from -872 to -744 m; (D) Salindres SD-101; (E) Les Vieilles Fumades - SC-1 and SC-2. 'AB' prefix and associated numbers refer to Alès Basin lithofacies description reported in Table 2. 'A' prefix and associated numbers refer to Alès, Saint-Chaptes and Issirac (ASCI) lake system lithofacies description detailed in Table 3.

and the well inclination. In the following text and figures, wells SC-1 and SC-2 have been merged into a single log. Furthermore, gamma-ray log and mud-logging analyses have been integrated to assess lithologies out of the cored intervals. The subsurface datasets (well logs, cores and cutting intervals) used in the present study are summarized in Table 1.

Sequence analysis

Analysis of vertical stacking patterns of sedimentary facies and stratigraphic surfaces identification have been performed, thus delineating depositional sequences which are defined as transgressive-regressive cycles (T-R sequence, *sensu* Embry & Johannessen, 1992). This sequence uses the subaerial unconformity as the unconformable portion of the boundary and the maximum regressive surface as the correlative conformity. This approach has practical interest since transgressive-regressive cycles can be defined in 1D from palaeoenvironmental interpretations of lithofacies and subaerial unconformities can be determined by the petrographic and diagenetic analysis of remarkable surfaces. In addition, this approach has proved to be relevant for linking the stratigraphic architecture and their controlling factors in other rift lake basins (e.g. Nutz *et al.*, 2017).

Palaeomagnetic measurements

Thirty-four sedimentary strata were sampled from Issirac Basin outcrops for the magnetostratigraphy. A total amount of 86 core-samples (25 mm in diameter) with measurable magnetizations were analyzed with intensities ranging from 10^{-5} to 10^{-4} Am⁻¹. Twenty-seven samples were subject to thermal stepwise demagnetization up to 620°C and 59 samples to alternating field stepwise demagnetization up to 100 mT. Palaeomagnetic measurements were performed using the superconducting rock magnetometer with on-line alternating field demagnetization system (760R; 2G Enterprises, Sunnyvale, CA, USA) at the CEREGE, Aix-en-Provence, France. Thermal demagnetization

was done using the furnace dedicated to Palaeomagnetic studies (MMTD80; Magnetic Measurements Limited, Aughton, UK). This oven is shielded in order to offer a heating chamber with a negligible ambient magnetic field. All data have been processed using the PaleoMac™ software (Cogné, 2003). Among the 86 samples, 54 samples were subject to palaeomagnetic interpretation allowing the determination of palaeomagnetic polarities in 27 sedimentary layers. For each sample, a tectonic dip correction has been performed prior to directional computations.

RESULTS

Lithofacies and depositional environments in the Alès depocentre

Fourteen lithofacies from Saint-Jean-de-Maruéjols-et-Avéjan (MAR-1 and MAR-101), Salindres (SD-101) and Allègres-les-Fumades (SC-1 and SC-2) (Fig. 4) wells have been characterized and classified based on both microfabrics and macrofabrics. The definition of lithofacies included criteria, such as: lithology, fossil content, petrographic characteristics, sedimentary structures and textural features. The lithological and petrographic characteristics, the sedimentary structures, the main diagenetic features and the composition of preserved biota for each depositional lithofacies from Alès Basin well-cores (AB1 to AB14) are summarized in Table 2 and illustrated in Figs 5, 6, 7 and 8. Lithofacies from Alès Basin well cores have been subdivided into four lithofacies categories: (i) carbonate-dominated lithofacies; (ii) mixed carbonate-terrigenous lithofacies; (iii) terrigenous-dominated lithofacies; and (iv) calcium sulphate lithofacies.

Carbonate-dominated lithofacies

Lithofacies AB1 - Brecciated nodular and clotted-peloidal limestones

Lithofacies AB1 is characterized by metre-scale, massive limestone beds characterized by nodulization and/or by clotted-peloidal texture (*sensu* Armenteros *et al.*, 1997) (Figs 5D, 5E and 6A to

Table 2. Definition and classification of the lithofacies identified from Alès Basin well cores (AB1 to AB14).

Code (Alès Basin)	Lithofacies	Lithology	Textural and sedimentary features	Diagenetic features	Fossil content	Figures
Carbonate-dominated lithofacies						
AB1	Brecciated-nodular and clotted-peloidal limestones	Limestone	1) Clotted-peloidal texture (sensu Armenteros et al., 1997); wackestone to packstone with subrounded micritic peloids (50 to 100 µm in diameter) and coated intraclasts. 2) Carbonate microbreccia: poorly sorted (10 to 1000 µm), angular to subangular micritic elements set within a micritic matrix or cemented by sparry calcite cements.	Subaerial exposure-related features are common, such as: root traces, anisopachous sparry calcite cements between micritized grains, circumgranular cracks and peloids with micritic bridges.	Gastropods (<i>Galba</i> , <i>Viviparus</i> and <i>Brotia</i>)	Figs 5D, 5E and 6A to 6D
Mixed carbonate-terrigenous lithofacies						
AB2	Fossiliferous marlstone and argillaceous marlstone	Whitish to greyish marlstone and argillaceous marlstone	Massive, structureless, homogeneous decimeter to meter-thick beds. Commonly interbedded within AB3 lignites.	-	Gastropods (<i>Galba</i> , <i>Viviparus</i> and <i>Brotia</i>), ostracods, bivalves, charophyte gyrogonites.	Fig. 5I
AB3	Lignite/coal interbedded in marlstone and clays	Lignite to organic-rich marlstone	Decimeter-thick, massive beds, transitional bedding contact, parallel laminations in marlstones.	Aragonitic shells are preserved.	Plant debris, freshwater gastropods with preserved aragonite (<i>Galba</i> , <i>Viviparus</i> , <i>Brotia</i>), ostracods, charophytes, phytoclasts remains and rare foraminifera.	Fig. 5C
AB4	Intraclastic floatstone	Argillaceous limestone	Floatstone with laminated endoclasts (microbial laminae?) embedded in an argillaceous bioclastic wackestone matrix.	-	Characean thalli and gyrogonites; ostracods, benthic foraminifers.	Figs 5F, 6E and 6F
AB5	Silty-argillaceous mudstone-wackestone with scattered bivalves and foraminifera	Argillaceous limestone	Dark, laminated argillaceous limestones (mudstone to wackestone texture) with variable carbonate and quartz silt fraction. Laminations are typically horizontal and parallel but convolute structures may occur.	-	Bivalves (<i>Polymesoda</i>), benthic foraminifers (<i>Textulariids</i>)	Figs 6G and 6H
AB6	Platy marlstones with scattered bivalves and foraminifers	Marlstone to calcareous marlstone.	Dark-grey platy marlstones and calcareous marlstones with horizontal, planar laminations.	-	Rare molluscs (<i>Polymesoda</i>), common coaly plant remains	Fig. 5A
AB7	Finely laminated, organic-rich marlstone	Marlstone.	Dark, finely laminated marlstone, with horizontal, planar laminations.	-	Unidentified organic debris	Fig. 5A
AB8	Bioturbated organic-rich argillaceous marlstone with abundant pyrite	Argillaceous marlstone.	Dark, bioturbated marlstone.	Common pyrite	Unidentified organic debris	Figs 6I and 6J
Terrigenous-dominated lithofacies						
AB9	Quartzose peloidal calcilutite	Quartzose calcilutite	Carbonate-mud-supported sediment containing various proportions of fine-to-coarse grained, subangular to subrounded quartz sand particles and peloids (=quartzose peloidal calcilutite or quartzose-peloidal wackestone.	-	Mainly ostracods, rare benthic foraminifera and mollusc fragments.	Figs 5G, 6K

AB10	Medium-to-coarse grained sandstone to quartzose calcarenite	Sandstone to quartzose calcarenite	to	1 to 10 cm thick flat-based beds of medium-to-coarse grained sandstones or quartzose calcarenites interbedded within quartzose calcilutites (AB9 lithofacies) or silty argillaceous limestones and marlstones (AB5-AB6 lithofacies). Allochems are essentially composed of quartz grains (40 to 60%) and calcitic peloids (40 to 60%). Deposits could be cross-bedded with mud draped foresets. Top of the beds often exhibits symmetric ripples in the Saint-Chaptes Basin.	Cements are completely lacking and the cohesion of the rock is mainly due to compaction.	Numerous plant debris	Figs 5H, 6L and 6M
-------------	---	------------------------------------	----	--	--	-----------------------	--------------------

Calcium-sulphate lithofacies

AB11	Planar to wavy-laminated mudstone/bindstone with sparse lenticular gypsum	Limestone to dolostone with gypsum (+ anhydrite relicts)	to	Planar to wavy laminated limestones and dolostone embedding sparse lenticular gypsum crystals, up to 0.3 mm in diameter (Fig 7A to B). They are found as: 1) polycrystalline secondary gypsum or anhydrite pseudomorphs, and 2) dissolution voids partially or entirely filled with calcite cement or bitumen. Gypsum spherulites are also present (Fig. 8F). The coalescence of lenticular gypsum crystal may lead to the formation of nodules (Figs 7A and 8G). Wavy laminations are partly related to displacive growth of gypsum within the sediment (Fig. 7A). However, preferential thickening of laminae at top of small-scale undulations and corrugations suggests a microbial original for such laminae.	(Early?) replacement of gypsum by anhydrite and later, partial transformation of anhydrite into gypsum, dissolution of anhydrite and/or gypsum, sparry calcite cements in molds.	Rare ostracods	Figs 7A, 7B, 8F and 8G
AB12	Planar to wavy-laminated mudstone/bindstone with vertical, elongated grass-like gypsum crystals	Dolostone and gypsum (+ anhydrite relicts)	to	Planar to wavy-laminated dolomicrites interbedded with layers of elongated (up to 1 cm long), subvertical, prismatic and smaller (<500 µm) lense-shaped gypsum crystals (Fig. 7C). The larger, grass-like elongated crystals exhibit relicts of an anhydrite precursor (Fig. 7E).	(Early?) replacement of gypsum by anhydrite and later, partial transformation of anhydrite into gypsum.	No identified biota	Figs 5B, 7C to E
AB13	Dolomitic mudstone with large, scattered, prismatic to elongated lenticular gypsum crystals	Dolostone and gypsum (+ anhydrite relicts)	to	Large (1-10 cm) prismatic to elongated gypsum crystals embedded in a structureless to planar-laminated dolomitic mudstone (Fig. 8D). Laminae are not disturbed around large crystals thus suggesting replacement of micrite into gypsum/anhydrite. Large crystals are dominantly composed of polycrystalline gypsum with rare relicts of anhydrite.	Crystals are commonly leached, filled with bitumen or replaced by dolomicrite.	No identified biota	Figs 7F, 7G and 8D
AB14	Irregularly laminated nodular gypsum/anhydrite alternating with laminated dolomicrite	Laminated gypsum (+ anhydrite relicts), dolomicrite laminae, native sulphur	to	Alternating planar-to-wavy laminar dolomicrite (1-10 mm thick intervals) and centimeter-thick layers of coalescent gypsum/anhydrite nodules (Figs 8A to C and 8E). Nodules mainly consists of secondary polycrystalline gypsum with rare relicts of anhydrite. Anhydrite/gypsum may be partially replaced by native Sulphur (Fig. 8C).	Partial transformation of anhydrite into gypsum. Partial replacement of anhydrite/gypsum by native sulphur. Fractures are common and are frequently filled with fibrous (satin spar) gypsum.	No identified biota	Figs 8A to C and 8E

6D). The brecciated limestones (Fig. 5D and E) are actually pseudobreccias comprising pseudoclasts bounded by circumgranular cracks or by a complex pattern of micrite-filled fractures. Lithofacies AB1 exhibits in some beds of clotted-peloidal fabrics which consist of poorly sorted grainstones composed of coarse-grained intraclasts with common micritic coating and smaller, poorly individualized peloids bounded together by micritic bridges (Fig. 6B and D). Root cracks (Fig. 5D and E), polygonal (desiccation) cracks and anisopachous calcite cements between micritized grains are also present within Lithofacies AB1 (Fig. 6A to D).

Interpretation: Brecciated-nodular and clotted-peloidal textures of lithofacies AB1 (Fig. 6A to E) characterize a palustrine environment at the margin of shallow lakes with fluctuating lake level (Freytet, 1973). The clotted-peloidal texture has been interpreted as corresponding to a more advanced degree of pedogenic transformation compared to the brecciated-nodular limestones (Armenteros *et al.*, 1997). The development of palustrine carbonates dominated by brecciated-nodular structures are known to mainly characterize semi-arid to intermediate climate environments (Platt & Wright, 1991). Similar lithofacies have been documented in the Issirac (Lettéron *et al.*, 2017) and Saint-Chaptes (Lettéron *et al.*, 2018) basins.

Mixed-carbonate-dominated lithofacies

Lithofacies AB2 - Fossiliferous marlstone and argillaceous marlstone

Lithofacies AB2 consists of whitish to greyish marlstone and argillaceous marlstone, organized into massive and structureless, decimeter to metre-thick beds. The macrofauna includes abundant gastropods (*Galba*, *Viviparus* and *Brotia*) and ostracods. Charophyte gyrogonites are common.

Interpretation: The occurrence of characean gyrogonites suggests a shallow (<10 m) lacustrine palaeoenvironment. In addition, the molluscan assemblage (*Galba*, *Brotia* and *Viviparus*) is indicative of very shallow (<2 m), freshwater to slightly brackish (<4‰) conditions (Daley, 1972) (Fig. 5I).

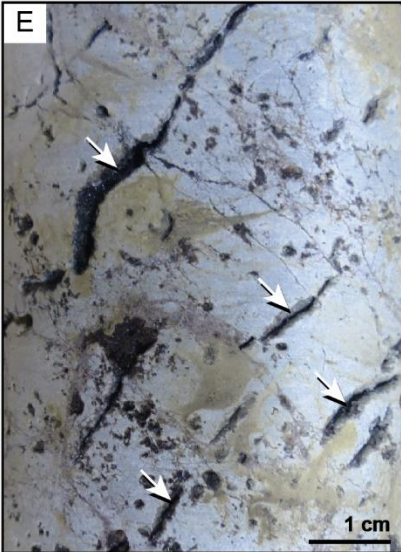
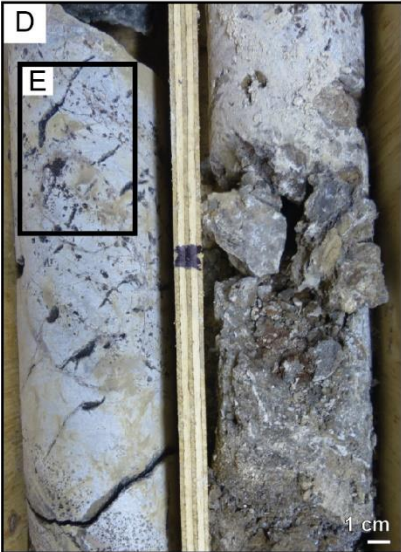
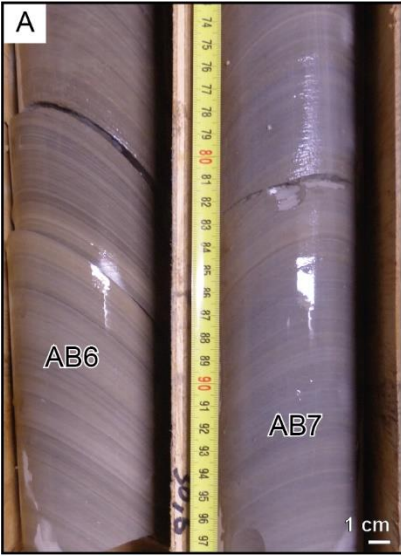


Fig. 5. Core photographs from Alès Basin well cores: (A) finely laminated dark-grey platy calcareous marlstone with horizontal, planar laminations (AB6 lithofacies) evolving to a finely laminated marlstone (AB7 lithofacies) (SC-1 well, -50.8 m); (B) dolostone with layers of planar to wavy-laminated gypsum and subvertical lens-shaped gypsum crystals (AB12 lithofacies) (MAR-1, -843 m); (C) coal layer intercalated between organic-rich marlstone layers (AB3 lithofacies) with some sparse charophyte gyrogonites (arrows) (SD-101 well, -605.8m); (D) carbonate microbrecciated and pedogenetized interval (AB1 lithofacies) (SC-1 well, -92 m); (E) zoom of (D) highlighting root traces and other pedogenetic features as root cracks (arrows) (AB1 lithofacies); (F) intraclastic floatstone (AB4 lithofacies); (G) quartzose calcilutite dominated interval (AB9 lithofacies) from SD-101 well (-830.5 m); (H) fine to coarse-grained sandstone (AB10 lithofacies) from SD-101 well (-700.3 m); (I) bivalve-rich fossiliferous marlstone (AB2 lithofacies) from SD-101 well (-386.3 m).

Lithofacies AB3 - Lignite and organic-rich marlstone

Lithofacies AB3 consists in up to 10 cm thick lignite beds alternating with brecciated, organic-rich marlstones (Fig. 5C). Lithofacies AB3 displays vertical transitional changes into fossiliferous marlstones AB2. The bioclastic fraction is significant and well-preserved. It includes gastropods (*Galba*, *Viviparus* and *Brotia*), bivalves, ostracods, characean gyrogonites and rarer benthic foraminifera.

Interpretation: Organic matter concentrations suggest oxygen-poor environments. Parallel laminations suggest a low energy depositional environment such as a coastal marsh (Samanta *et al.*, 2016). Such an interpretation is also supported by the common occurrence of pedogenic features (root traces) within or above the lignite beds. Similar to facies AB2, the molluscan assemblage (*Galba*, *Brotia* and *Viviparus*) is indicative of freshwater to slightly oligohaline palaeoenvironments.

Lithofacies AB4 - Intraclastic floatstone

Lithofacies AB4 is a floatstone with laminated intraclasts (stromatolites) embedded within an argillaceous bioclastic wackestone matrix (Fig 5F). Characean stems and gyrogonites are commonly trapped within microbial laminae (Fig. 6E) which are also present in matrix (Fig. 6F). Ostracods and benthic foraminifera are other significant biota present in AB4 lithofacies.

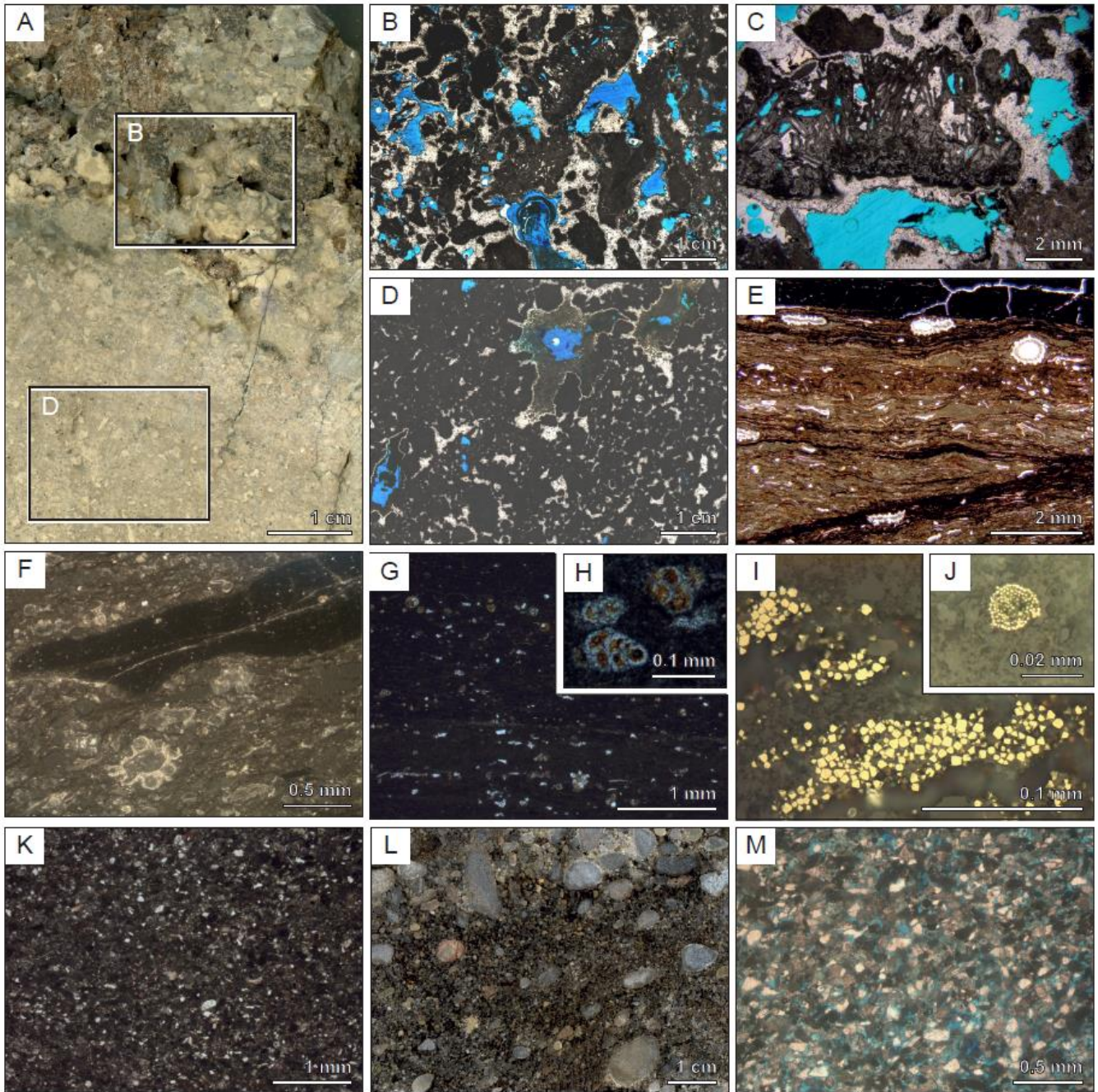


Fig. 6. (A) Core photograph of a nodular carbonate breccia (AB1 lithofacies), SC-2 well. (B), (C) and (D) Thin-section microphotographs under polarized light microscopy of pedogenic, nodular carbonate breccia (AB1 lithofacies), showing micritized grains with anisopachous calcite cements - (B) and (C) - or peloids with micritic bridges (D), SC-2 well. (E) and (F) Thin-section microphotographs under polarized light microscopy of a floatstone with reworked, rounded intraclasts (laminated soft pebbles), and characean stems within matrix (AB4 lithofacies), SC-2 well. (G) and (H) Thin-section microphotographs incident light of a laminated, silty-argillaceous mudstone-wackestone with scattered ostracods, mollusc fragments and foraminifera (AB5 lithofacies) (for example, -900 m - MAR-1 well). (I) and (J) Thin-section microphotograph under reflected light of an organic-rich, argillaceous marlstone (AB8 lithofacies) with abundant cubic framboidal pyrite (for example, -694 m - MAR-1 well). (K) Quatzose peloidal calcilutite (AB9 lithofacies), thin-section microphotograph, polarized light, SC-2 well. (L) Core photograph of a poorly sorted sandstone and conglomerate (=Célas Sandstone) (AB10 lithofacies). (M) Fine to medium-grained quatzose calcarenite (=Célas Sandstone) (AB10 lithofacies), thin-section microphotographs under polarized light, SC-2 well.

Interpretation: Common occurrences of characean, textulariids and *Polymesoda* may suggest deposition in mesohaline and relatively shallow-waters (e.g. Daley, 1972) or may be related to sediment transport from a neighbouring marginal lake area. In lithofacies AB4 (Fig. 5F), the occurrence of microbial bindstone lithoclasts embedded in characean-rich wackestone is indicative of reworking in shallow-water, coastal lacustrine environments.

Lithofacies AB5 and AB6 - Silty-argillaceous mudstone-wackestone with scattered molluscs and benthic foraminifera (AB5) and platy marlstones with scattered bivalves and foraminifera (AB6):

Lithofacies AB5 consists of a dark grey, laminate argillaceous limestone (mudstone to wackestone texture) with variable carbonate and quartz silt fraction. Laminations are typically horizontal and parallel but convolute structures may occur. Bivalves (*Polymesoda*), ostracods and benthic foraminifera (textulariids) represent the dominant biota (Fig. 6G and H). Lithofacies AB5 may form a thick (ca 120 m in MAR-1) and monotonous succession or may be organized into metre-thick beds interbedded within AB2 fossiliferous marlstones (SD-101) (Fig. 4A and C).

Lithofacies AB6 is composed of dark-grey platy marlstones and calcareous marlstones with horizontal, planar laminations (Fig. 5A). Bioclasts are rarer than in AB5 lithofacies and mostly consist of bivalves (*Polymesoda*), ostracods and benthic foraminifera. Platy marlstones are organized into metre to decametre-scale intervals (up to 50 m thick in MAR-1: Fig. 4A) interbedded with organic-rich marlstones (AB7) and argillaceous marlstones (AB8).

Interpretation: The preservation of organic matter as well as lamination in lithofacies AB6 suggests relatively poorly oxygenated waters and is likely to be responsible for the limited benthos on the lake bottom (Gierlowski & Rust, 1994). Lithofacies AB6 has also been reported in the Priabonian from the Saint-Chaptes Basin by Lett eron *et al.* (2018) and interpreted as a perennial lake lithofacies. Lithofacies AB5 and AB6 deposited in brackish lake settings under water depths slightly deeper than those associated with lithofacies AB2 and AB3.

Lithofacies AB7 and AB8 - Organic-rich marlstone (AB7) and argillaceous marlstone (AB8):

Lithofacies AB8 consists of a dark, finely laminated marlstone, with horizontal, planar laminations (Fig. 5A). This lithofacies differs from AB6 by its higher organic matter content and by its total absence of preserved calcified biota. Lithofacies AB8 is a bioturbated, dark, organic-rich argillaceous marlstone forming metre to decametre-thick intervals which commonly alternate with AB6 and AB7. Significant concentrations of framboidal pyrite (<50 µm in diameter) are particularly abundant in this lithofacies (Fig. 6I and J). Similar to AB7, it is completely devoid of calcified biota.

Interpretation: The preservation of high concentrations of organic matter and the abundance of pyrite suggest oxygen-poor conditions within the hypolimnion of a permanent, stratified lake and probably the action of bacterial sulphate reduction processes (e.g. Raiswell *et al.*, 1988; Talbot, 1988; Ellis *et al.*, 2015) (Fig. 6I and J). The lack of preserved metazoans such as molluscs may indicate profundal (>10 m) and/or low oxygenation conditions. Even though argillaceous, clay-rich deposits ('black shales') are assigned to low-oxygen environments, some worms have been shown to adapt to such unfavourable conditions and to form significant bioturbation (Lobza & Schieber, 1999) such as that observed in lithofacies AB8. Finally, the lack of subaerial exposure evidence (desiccation and pedogenesis), erosional features and the horizontal planar laminations within intervals dominated by mixed carbonate-terrigenous lithofacies (AB2 to AB8) suggest deposition in a perennial, low energy water body.

Terrigenous-dominated lithofacies

Lithofacies AB9 and AB10 - Peloidal quartzose calcilutite (AB9) and Medium to coarse-grained sandstone to quartzose calcarenite (AB10):

Lithofacies AB9 is a mud-supported sediment containing various proportions of fine to coarse-grained, subangular to subrounded quartz sand particles and carbonate grains such as peloids and

limestone lithoclasts (=quartzose peloidal calcilutite or quartzose-peloidal wackestone) (Figs 5G and 6K). Ostracods, bivalves (*Polymesoda*) and benthic foraminifera (textulariids) occur within AB9 lithofacies. AB9 is typically found interbedded within AB10 quartzose sandstones/calcarenites (Fig. 4D and E).

Lithofacies AB10 forms 1 to 10 cm thick flat-based beds of medium to coarse-grained sandstones or quartzose calcarenites interbedded within quartzose calcilutites (AB9 lithofacies) or silty argillaceous limestones and marlstones (AB5 and AB6 lithofacies) (Fig. 5H). Allochems are essentially composed of quartz grains (40 to 60%) and calcitic peloids (40 to 60%). Scattered quartz pebbles (<1 cm) may occur within the AB10 sandstones (Fig. 6M). Symmetrical ripples are common. Cements are completely lacking, and the cohesion of the rock is mainly due to compaction (Fig. 6L).

Interpretation: The lack of matrix in lithofacies AB10 sediments and the occurrence of symmetrical wave ripples suggest a deposition in a lacustrine shoreface environment. The high proportion of quartz grains (40 to 60% of the sand-size grains) suggests a lacustrine shoreface area subject to significant terrigenous supplies. In contrast, the high carbonate mud content in lithofacies AB9 suggests low energy environments (below wave base) and/or development of subaqueous grass meadows on the lake bottom (Lettéron *et al.*, 2018). The occurrence of benthic foraminifera and *Polymesoda* is indicative of brackish water palaeoenvironments. Lithofacies AB9 and AB10 are interpreted to have been deposited in a shallow-water area of a brackish lacustrine delta.

Calcium sulphate lithofacies

Lithofacies AB11 - Planar to wavy laminated mudstone/bindstone with sparse lenticular gypsum

Lithofacies AB11 consists of planar to wavy laminated limestones and dolostone embedding sparse lenticular inclusions, up to 0.3 mm in diameter (Fig. 7A and B) which are made of polycrystalline secondary gypsum or anhydrite. Occasionally, such lens-shaped inclusions are leached and

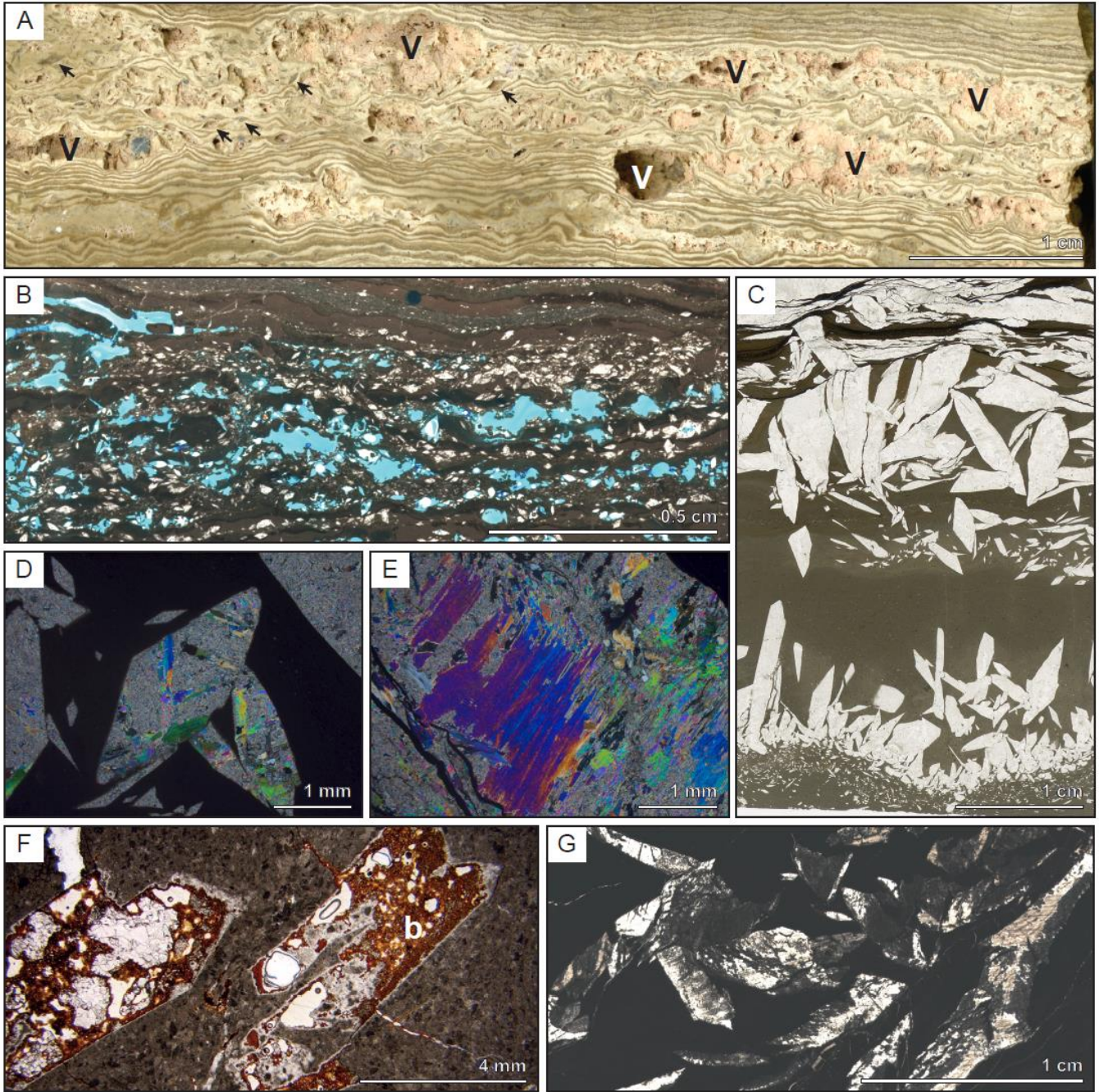


Fig. 7. (A) Planar to wavy laminated bindstone with displacive lenticular gypsum (AB11 lithofacies) showing large dissolution voids (v), SC-1 well. (B) Thin-section microphotographs under polarized light, showing sparse lenticular gypsum crystals interbedded in a millimetre-scale wavy laminae (AB11 lithofacies), SC-1 well. (C) Thin-section photograph of elongated, prismatic gypsum crystals alternating with dolomitic layers (for example, 105.7 m - SC-2 well) (AB12 lithofacies). (D) and (E) Thin-section microphotograph under crossed polars showing relicts of anhydrite precursor (high-order birefringence colors) within lithofacies AB12, SC-1 well. (F) and (G) Thin-section microphotographs under polarized light of dolomitic mudstone with large prismatic to elongated lenticular gypsum (AB13 lithofacies); SC-2 well: (F) leached prismatic gypsum crystals filled with bitumen (b); and (G) elongated lenticular gypsum crystals partially replaced by dolomicrite.

dissolution voids are partially or entirely filled with calcite cement or bitumen. Gypsum spherules are also present (Fig. 8F). The coalescence of lenticular gypsum crystals may lead to the formation of nodules (Figs 7A and 8G). Wavy laminations are partly related to displacive growth of gypsum within the sediment (Fig. 7A). However, preferential thickening of laminae at top of small-scale undulations and corrugations suggests a microbial origin for such laminae. Rare ostracods are trapped within the carbonate laminae.

Interpretation: The displacive growth of small lenticular gypsum crystals suggests a formation a few centimetres below the sediment-water interface (Truc, 1978). Such evaporitic lithofacies are interpreted to have been deposited in a shallow marginal calcium sulphate lake (Truc, 1978; Ortí, 1997). Additionally, gypsum spherules have been shown to form in subaqueous environments (Vogel *et al.*, 2010). Sparse lenticular gypsum crystals embedded within microbial carbonate laminae are common in Palaeogene evaporite basins from Western Europe (e.g. Truc, 1978; Ortí, 1997; Dromart & Dumas, 1997).

Lithofacies AB12 and AB13 - Planar to wavy laminated mudstone/bindstone with vertical, elongated, prismatic gypsum crystals (AB12) and dolomitic mudstone with large, scattered, prismatic to elongated lenticular gypsum crystals (AB13):

Lithofacies AB12 is composed of planar to wavy-laminated dolomicrites alternating with layers composed of elongated (up to 1 cm long), subvertical, prismatic gypsum crystals associated with smaller (<500 µm) lens-shaped gypsum crystals (Figs 5B and 7C). The larger, prismatic elongated crystals exhibit relicts of an anhydrite precursor (Fig. 7E). Observations under optical microscopy failed to find any preserved biota.

Lithofacies AB13 is composed of large (1-10 cm) prismatic to elongated gypsum crystals embedded in a structureless to planar-laminated dolomitic mudstone (Fig. 8D). Laminae are not

disturbed around large crystals, thus suggesting replacement of micrite into gypsum/anhydrite. Large crystals are dominantly composed of polycrystalline gypsum with rare relicts of anhydrite. Occasionally, crystals are leached and filled with bitumen (Fig. 7F) or replaced by dolomicrite (Fig. 7G).

Interpretation: Grass-like gypsum crystals (AB12 lithofacies, Figs 5B and 7C) are known to develop just beneath the sediment-water interface during very early diagenesis and are able to protrude above the sediment surface (Truc, 1978). The modern analogues of such gypsum growth forms are hummocky crusts of selenite gypsum reported from various salt pan environments (Ortí *et al.*, 1984). Large and scattered, prismatic to elongated lenticular gypsum (after anhydrite alteration) within homogeneous dolomicrite (AB13 lithofacies) are likely to form during early diagenesis replacing carbonate mud. As evidenced in modern saline lake environments, dolomicrite may have resulted from syn-depositional microbially-induced processes (Corzo *et al.*, 2005).

Lithofacies AB14 - Irregularly laminated nodular gypsum/anhydrite alternating with laminated dolomicrite

Lithofacies AB14 consists in alternating horizontal to wavy laminar dolomicrite (1-10 mm thick intervals) and centimetre-thick layers of coalescent gypsum/anhydrite nodules (Fig. 8A to C and E). Nodules mainly consists of secondary polycrystalline gypsum with rare relicts of anhydrite. Anhydrite/gypsum may be partially replaced by native sulphur (Fig. 8C).

Interpretation: In non-marine evaporitic environments, nodular gypsum and anhydrite have been interpreted to result from early diagenetic transformation of a laminated gypsum precursor which formed in perennial lake environments, during a drying ('sabkhatization') phase of the saline lake (Hussain & Warren, 1989; Salvany *et al.*, 1994). Similar to the Alès Basin, in other Palaeogene continental evaporite basins from France and Spain, laminated-nodular gypsum alternations have

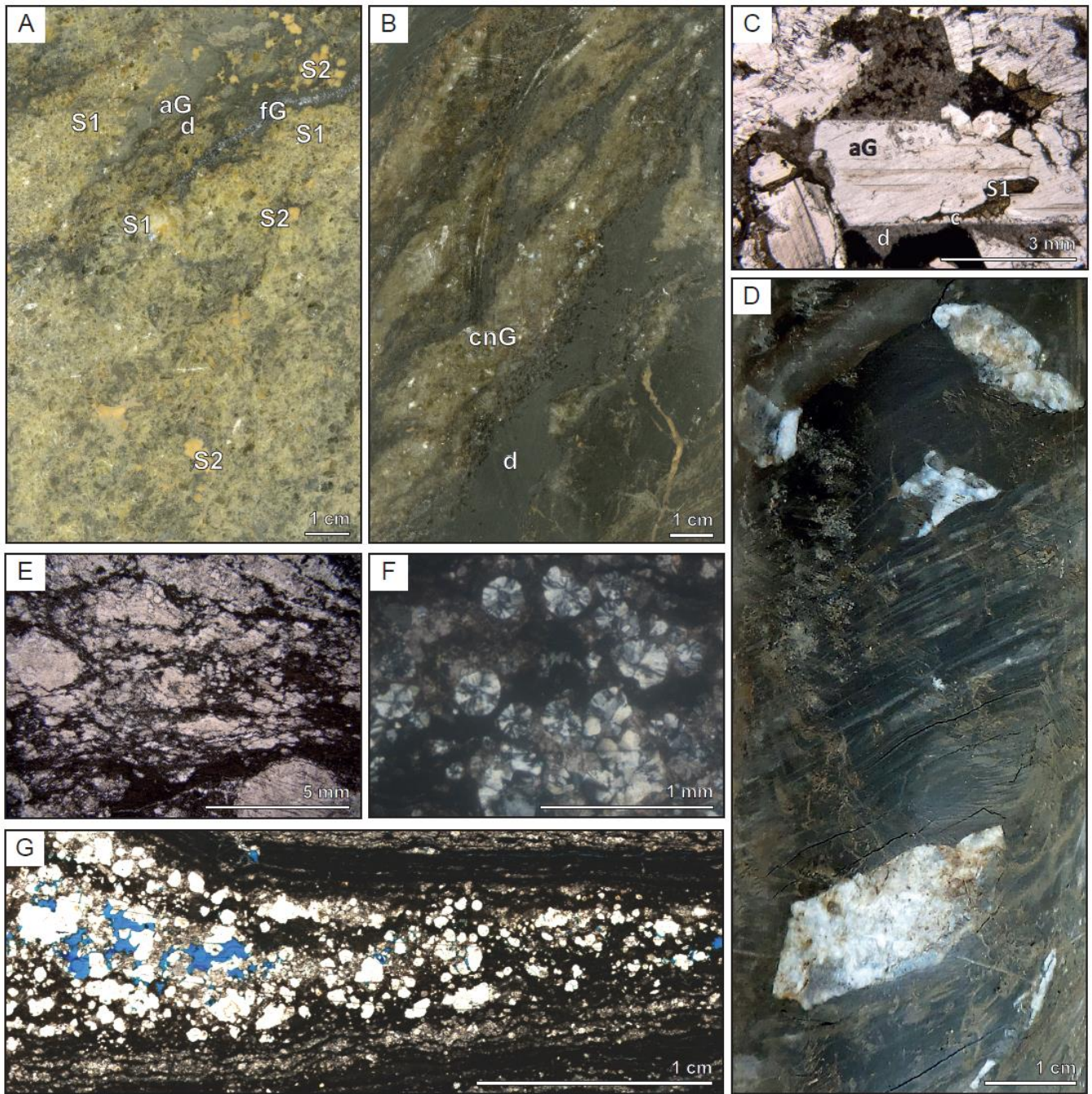


Fig. 8. (A) Laminated-nodular beds of gypsum/anhydrite alternating with laminated dolomicrite (AB14 lithofacies), core photograph, SC-2 well; aG: anhedral, polycrystalline gypsum; fG: fibrous gypsum in fracture; d: dolomicrite/organic matter laminae; S1: native sulphur replacing gypsum (light yellow); S2: native sulphur cement (occluding pores) (dark yellow). (B) Core photograph showing coalescent nodules of gypsum (cnG) interbedded within dolomicrite (d) layers (AB14 lithofacies), SC-1 well. (C) Thin-section microphotograph under polarized light showing the partial replacement of gypsum (aG) by native sulphur (S1) and by sparry calcite on the periphery of the gypsum crystal (c); the matrix embedding gypsum crystals is made of dolomicrite (d), SC-2 well. (D) Core photograph of organic-rich, dolomitic mudstones with large, scattered, prismatic gypsum crystals (AB13 lithofacies), SC-2 well. (E) Thin-section microphotograph under polarized-light of nodular gypsum alternating with dolomicrite layers (AB14 lithofacies), well SC-1. (F) Detail under crossed polars of gypsum spherulites, well SC-1. (G) Thin-section microphotograph of a planar-laminated bindstone with displacive lenticular and spherulitic gypsum (AB11 lithofacies), well SC-1.

been reported from the central parts of the lake areas (Ortí & Salvany, 1997; Arenas & Pardo, 1999) and are related to repeated changes in lake levels (subaqueous to playa/sabkha stages). The occurrence of anhydrite relicts within nodular gypsum lithofacies strongly suggests that such nodules have undergone rehydration processes from an anhydrite precursor (e.g. Shearman, 1966; Truc, 1978). However, such nodular anhydrite precursors may have themselves derived from early diagenetic (Shearman, 1983), or late burial replacement (Loucks & Longman, 1982) of gypsum. Additionally, the presence of native sulphur replacing gypsum (Fig. 8A) may result from (bacterial?) sulphate reduction processes during early stages of diagenesis in an organic-rich and anoxic environment.

Transgressive-Regressive cycles in the Alès depocentre

Saint-Jean-de-Maruéjols-et-Avéjan wells: MAR-1 and MAR-101

In MAR-1 well (Fig. 4A), the Priabonian carbonate succession overlies at -1299 m, microconglomerates with reworked Cretaceous elements and micritic matrix that may be interpreted as continental Bartonian deposits as those observed in the Saint-Chaptes Basin (Robiac mammal fossil site) and dated MP16 by Rémy (2015). The early Priabonian interval (-1299 to -1110 m) is characterized by an upward transition from marlstones (AB6-8) to evaporitic deposits (AB11 to AB14) thus suggesting a lake regression. Above, a return to non-evaporitic, perennial lacustrine deposits are indicative of a lacustrine transgression whose maximum is possibly recorded by a 30 m thick interval of organic-rich marls (920-950 m). A second regressive stage is evidenced by the increasing upward development of evaporitic facies (AB11 to AB14) up to 820 m. In MAR-101 (Fig. 4B and C), the top of the upper evaporitic interval has been cored (Fig. 4B: -822 m). The surface is a conformable and sharp contact between millimetre-scale gypsum/anhydrite dolomicrite alternation (AB14) and marlstones (AB6). The lack of dissolution features within AB14 facies suggests that the evaporitic interval has not

been affected by subaerial exposition. Above (up to -680 m in MAR-1), an upward transition from calcareous marlstones (AB6) to organic-rich argillaceous marlstones (AB7), occurs and suggests a transgressive trend. The latest Priabonian succession is made of two intervals (-680 to -495 m and -495 to -430 m) displaying a vertical lithofacies change from palustrine lignite-rich deposits to ostracod and foraminifera-rich lacustrine argillaceous limestones (AB3 and AB5) which strongly suggest two transgressive hemicycles which are topped by an exposure surface. Priabonian deposits are sharply overlain by siliciclastic deposits (siltstones, sandstones and conglomerates) assigned to Late Oligocene (Alabouvette *et al.*, 1983; Frédet, 1987; Bonnet *et al.*, 2011).

Salindres well: SD-101

In SD-101 well (Fig. 4D), evaporitic deposits (AB11 to AB14: -980 to -920 m) overlie reddish conglomerates and claystones of possible late Cretaceous to Palaeocene age. The overlying interval (-920 to -613 m) displays an upward transition from calcareous marlstones and marlstones AB6 and AB7 (transgressive stage) to alternating silty marlstone and sandstones (AB7, AB9 and AB10). The occurrence of characean gyrogonites at -613 m and -615 m suggests very shallow-water environments at the top of this interval and the infill of the lake depocentre by terrigenous sediment (normal regressive stage). The latest Priabonian deposits consists of a succession of two intervals (-613 to -490 m and -490 to -290 m) displaying a vertical lithofacies change from lignite-rich deposits with freshwater molluscs to ostracod and foraminifera-rich lacustrine argillaceous-silty marlstones to limestones (AB2 and AB3) which are interpreted, similar to the MAR-1 well, as representing two transgressive hemicycles. As observed in MAR-1 well, Priabonian lacustrine carbonates are sharply overlain by siliciclastic deposits (siltstones, sandstones and conglomerates) of Oligocene age.

Allègre-les-Fumades: SC-1 and SC-2 wells

In Fig. 4E, wells SC-1 and SC-2 have been merged into a single log. The base of the Priabonian succession is not reached in SC-1. The base of core SC-1 consists of organic-rich silty marlstones (AB8) that are overlain by a 20 m thick evaporitic interval (AB11 to AB14), thus suggesting a regressive pattern (forced regression). Above this lower calcium sulphate-rich interval, SC-1 cores display a thick vertical upward succession (>130 m) from calcareous marlstones and argillaceous limestones (AB6) to organic-rich argillaceous marlstones (dominantly AB7 and AB8) which is indicative of a transgressive pattern. The lower part of SC-2 exhibits a vertical transition from calcareous marlstones and argillaceous limestones (AB6) to a 25 m thick interval of interbedded carbonates (dolostone and limestone) and calcium sulphates (gypsum and anhydrite) (AB11, AB13 and AB14) which correspond to a stage of forced regression of the lake. The top of this interval is highly karstified (-86 m) which suggests a subaerial exposition of the basin after the deposition of calcium sulphates. The karstified interval is overlain by pedogenetized nodular and brecciated carbonates (AB1: Fig. 4E) and marks a new lacustrine transgression. Above (-76 to -12 m), the vertical upward succession from organic-rich argillaceous mudstones (AB8) to medium to coarse-grained sandstones (AB9 and AB10) suggests the progradation of a siliciclastic depositional system into the ASCI lake and a normal regressive pattern.

Magnetostratigraphy (Issirac Basin)

Regarding the low quality of the palaeomagnetic data and considering the low deformation of the sedimentary cover, no fold test could be performed. However, four types of demagnetization patterns were evidenced (Fig. 9): 12 samples are characterized by one single component of normal polarity (Type 1), 16 samples show clear and stable reverse polarities with a slight normal overprint (Type 2), 22 samples display a great single pattern which characterizes large coercivity overlap of a normal soft component over a reverse component, more resistant to alternating field demagnetization (Type 3). In addition, four samples show intermediate directions with, for most of them, high resistance

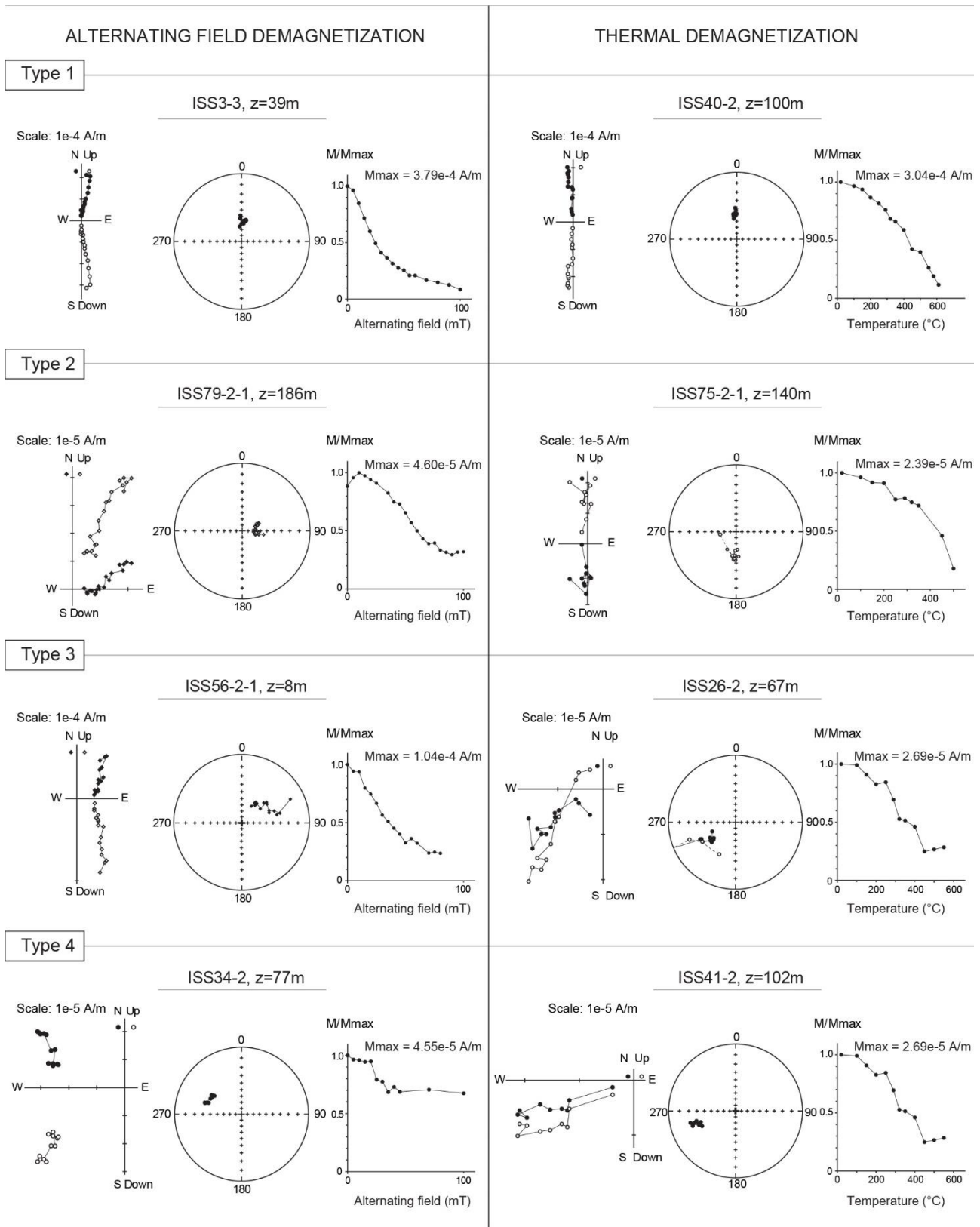


Fig. 9. Alternating field (to the left) and thermal (to the right) demagnetization for samples displaying the four types of demagnetization pattern: normal polarity (type 1), reverse polarity (type 2), great circle pattern (type 3) and intermediate polarity (type 4).

to alternating field demagnetization (Type 4). The tracing of partial and/or total remagnetization must therefore be carefully discussed. Palaeomagnetic results presenting **great** circles (Type 3 in Fig. 9) were interpreted as primary reverse polarities with large but not full normal remagnetization of the carbonates during diagenesis. Most of the normal polarities present relatively strong magnetizations (several 10^{-4} Am⁻¹, Type 1 in Fig. 9) which can be also attributed to the acquisition of a secondary magnetization carried by magnetic minerals formed during diagenesis or brought by fluid circulation in the pore network (e.g. Elmore *et al.*, 2012, and references therein). The palaeomagnetic data and polarity interpretations for each sample are provided in the **Supplementary Material - Table**.

Most of the interpretable layers display a primary record of a reverse polarity. The few layers in which only normal polarities were observed are isolated within the sedimentary column and are far from identified sedimentary discontinuities. According to the Geomagnetic Polarity Time Scale (Ogg, 2012), no short-interval of normal polarity is expected in the considered time interval. Consequently, those layers also suffer from remagnetization acquired during a normal polarity period. The palaeomagnetic results of the entire sedimentary column are interpreted as resulting from the record of a primary reverse polarity (Fig. 10A).

The charophyte oogones identified in the Issirac Basin (Lettéron *et al.*, 2017) suggest that all of the studied interval fits within the late Priabonian to early Rupelian *Harrisichara tuberculata* Superzone (Riveline, 1996). On the basis of the reconstructed geomagnetic polarity record (Fig. 10A) and charophyte markers (Fig. 10B and C), four possible polarity scales were proposed (Fig. 10A): only reverse polarities (C13r) and no depositional hiatus (hypothesis 1); only reverse polarities (C13r and C12r) and one major depositional hiatus which includes C13n chron (hypotheses 2 and 3); or only reverse polarities (C12r) and no depositional hiatus (hypothesis 4).

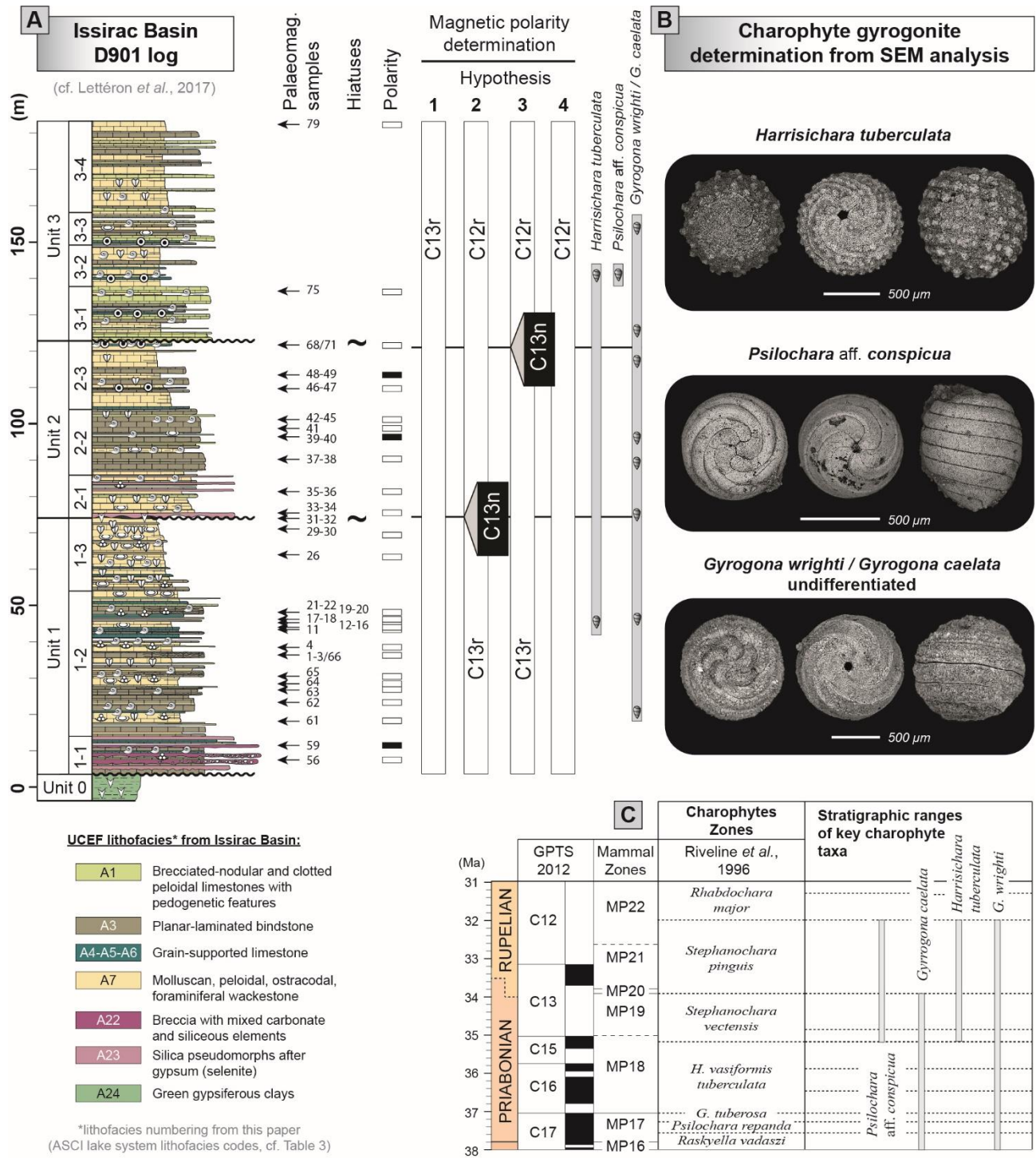


Fig. 10. Magnetostratigraphic interpretations of the Issirac Basin palaeomagnetic dataset. (A) The reference Geomagnetic Polarity Time Scale used to attribute polarity chron to our magnetostratigraphic scale is derived from Ogg (2012). Three distinct interpretations are consistent with the available biostratigraphic constraints from the studied D901 section from Issirac Basin. (B) Charophyte gyrogonite scanning electron microscopy (SEM) pictures and determinations from Lettéron et al. (2017). (C) Temporal distribution of key charophyte taxa from charophyte zonations of Riveline et al. (1996) and identified chronostratigraphic time interval attributed to Issirac samples (horizontal grey bar). UCEF: Upper Carbonate and Evaporite Formation, sensu Lettéron et al. (2018).

IMPLICATIONS FOR THE ALÈS, SAINT-CHAPTES AND ISSIRAC LAKE SYSTEM

Synthesis of depositional environments in the Alès, Saint-Chaptes and Issirac lake system

The integration of Alès Basin lithofacies (this paper cf. *Lithofacies and depositional environments in the Alès depocentre* section) with those previously defined from Issirac (Lettéron *et al.*, 2017) and Saint-Chaptes (Lettéron *et al.*, 2018) basins led to the definition of a generalized lithofacies classification (A1 to A28) for the Priabonian ASCI lake system which integrates both lake depocentre and lake margin area. The proposed classification and corresponding palaeoenvironmental interpretations are summarized in Tables 3 and 4, and reported in Figs 4 and 10. Nine lithofacies associations ranging from palustrine to profundal lake depositional environments have been identified: (i) carbonate-dominated lithofacies associations: palustrine (FA1), shallow lake or littoral (FA2); (ii) mixed carbonate-terrigenous lithofacies associations: wetlands (ponds, swamps and marshes) (FA3), lacustrine coastal mud-flat (eulittoral) (FA4), infralittoral lake (FA5), profundal lake (FA6); (iii) terrigenous dominated lithofacies association: fluvio-deltaic (FA7); and (iv) calcium sulphate dominated lithofacies associations: dry mud-flat or shallow saline pan (FA8) and saline lake (FA9).

Carbonate-dominated facies associations

Facies Association 1 – Palustrine facies association – FA1 consists of brecciated limestones characterized by nodulization or by clotted-peloidal texture (A1 lithofacies) (Fig. 6A to D) (*sensu* Armenteros *et al.*, 1997) and less frequently by, thinly-bedded oncolitic to bioclastic grainstones (A2 lithofacies). Subaerial exposure-related features are common, such as: root traces, polygonal (desiccation) cracks, anisopachous calcite cements between micritized grains (Fig. 6B and C), circumgranular cracks and peloids with micritic bridges (Fig. 6D). Pedogenic transformations result in ^{13}C -depleted isotope signatures as observed in the Saint-Chaptes Basin by Lettéron *et al.* (2017) (-4.94 to -5.35 $\delta^{13}\text{C}_{\text{V-PDB}}$) and in the Issirac Basin by Lettéron *et al.* (2018) (-1.75 to -6.93 $\delta^{13}\text{C}_{\text{V-PDB}}$) (e.g. Gierlowski-Kordesch, 2010). FA1 deposits commonly interfingered with shallow lacustrine FA2.1

intervals, thus suggesting high-frequency lake level variations in the Issirac Basin (Lettéron *et al.*, 2017). In the subunit U3.1 of the Issirac Basin, thick intervals of FA1 (up to ca 1.8 m) are found associated with gastropods thriving in shallow freshwater environments (*Galba longiscata*, *Brotia albigensis* and *Viviparus soricinensis*).

Table 3. Definition and classification of the Alès, Saint-Chaptes and Issirac (ASCI) lake system lithofacies (A1 to A28) identified from Alès Basin well cores, and from Issirac (Lettéron *et al.*, 2017) and Saint-Chaptes outcrops (Lettéron *et al.*, 2018).

Code (ASCI lake system)	Lithofacies	Lithology	Textural and sedimentary features	Diagenetic features	Fossil content
FA1 - Palustrine					
A1	Brecciated-nodular and clotted-peloidal limestones	Limestone	1) Clotted-peloidal texture (sensu Armenteros <i>et al.</i> , 1997): wackestone to packstone with subrounded micritic peloids (50-100 µm in diameter) and coated intraclasts. 2) Carbonate microbreccia: poorly sorted (10-1000 µm), angular to subangular micritic elements set within a micritic matrix or cemented by sparry calcite cements.	Subaerial exposure-related features are common, such as: root traces, anisopachous sparry calcite cements between micritized grains, circumgranular cracks and peloids with micritic bridges.	Gastropods (<i>Galba</i> , <i>Viviparus</i> and <i>Brotia</i>)
A2	Thinly bedded oncolithic-bioclastic grainstone	Limestone	Poorly sorted grainstones to rudstones with oncoids (0.1-5 mm in diameter). Decimetre-thick lenticular beds (lense lateral extension <100 m) interbedded within A12. Oncoids are generally small-sized (<2 mm) and the nucleus of the oncoids is generally not preserved and occurs as molds. The shape of most of the nucleus sections are rounded and elongated. The cortex is generally made of regular, continuous, relatively isopachous micrite laminae. No erosional feature at the base of beds.		Molluscs, ostracods and well-preserved benthic foraminifers (miliolids and textulariids)
FA2 - Shallow lake or littoral					
A3	Planar-laminated bindstone	Limestone	Laminated limestones with bindstone texture that are dominantly made of sub-horizontal, wavy, clotted peloidal micrite laminae (100 µm to 1 mm thick) alternating with variably continuous microsparite to sparite laminae (up to 0.5 mm thick). Common desiccation cracks. Wavy micritic laminae are commonly found draping mollusk shells, ostracods or characean gyrogonites.	Cementation of calcite spar/microspar occurs in the fenestral pores.	Ostracods, molluscs (<i>Potamides</i> , <i>Polymesoda</i> , <i>Galba</i>), charophyte gyrogonites and thalli, rare organic phytoclasts
A4	Peloidal packstone-grainstone with abundant molluscs, ostracods and benthic foraminifera	Limestone	Moderately to well-sorted packstone-grainstone with abundant peloids and benthic foraminifers. Cm to dm-thick limestone beds. Beds are devoid of significant sedimentary structure.	Formation of calcite spars occurs in the intergranular pore space. Peloids do not show evidences of significant mechanical or chemical compaction.	Micritic mollusk bioclasts (<i>Potamides</i> - <i>Polymesoda</i> association). Rare foraminifera and ostracods
A5	Ooidal packstone-rudstone	Limestone	Well to moderately-sorted oolitic grainstone. Decimeter thick tabular limestone beds displaying irregular base and top surfaces as well as cross-bedding structures. Ooids developed around bioclasts (ostracods shells or mollusk debris) or rarely mineral grains (quartz) and are commonly moderately micritized.	Limited mechanical compaction. Limited calcite cementation.	Charophyte gyrogonites, ostracods, rare molluscan debris

A6	Molluscan grainstone-rudstone (= coquina)	Limestone	Dense accumulation of recrystallized or leached, partly fragmented bivalve shells (<i>Polymesoda</i>) set in a micritic or peloidal matrix. Cm to dm-thick limestone beds, showing irregular laminations. Inverse grading sequences and erosive bases.	Calcite cementation	spar/microspar	Gastropods and monospecific community of pelecypods (<i>Polymesoda</i>)
A7	Peloidal mudstone-wackestone with molluscs, ostracods and benthic foraminifera	Limestone	Well stratified centimeter-thick (1 to 10 cm) beds to massive 10 m-thick intervals of micritic limestones., Mudstone to wackestone texture commonly displaying accumulation of <i>Polymesoda</i> , ostracods, benthic foraminifera and scattered macrofossils (molluscs) that are set in a dark homogeneous micrite.	Intraskelatal space of molluscs is commonly filled with geopetal accumulations of rounded to elongated peloids whose diameter ranges from 100 to 400 µm. The original shape of the well-sorted pellets is only preserved in the sheltered intraskelatal voids. Mechanical compaction of soft peloids.		Monospecific composition of pelecypods (<i>Polymesoda</i>) often articulated and showing lack of physical abrasion, Ostracods (valves closed), diversified foraminifera (Miliolida, Rotalida, Textularida), gastropods, rare charophyte debris and organic phytoclasts.
A8	Silty claystones with sideritic rhizoconcretions	Silty clays	Decimeter to meter-thick beds of silty clay with reddish-orange colored sideritic rhizoconcretions. Vertical concretions are randomly spreading within the silty clays.	Pedogenic rhizoconcretions.	sideritic	No identified biota
A9	Very fined-grained quartz-rich peloidal packstone-grainstone		Mixture of carbonate allochems (dominantly peloids with rarer ostracods and molluscs) and very fine to fine-grained quartz particles (up to 25%) that are set in a matrix made of carbonate silt particles, micrite and clays (80% I/S RO, 9-17% illite, <8% kaolinite and <5% chlorite). Deposits are organized into dm-thick strata displaying symmetric ripple structures. Interbedded with A10 facies. More rarely, some beds exhibit an erosive base.			Rare ostracods and molluscs
A10	Fossiliferous marlstone and argillaceous marlstone	Whitish to greyish marlstone and argillaceous marlstone	Massive, structureless, homogeneous decimeter to meter-thick beds. Commonly interbedded within A12 lignites.	-		Gastropods (<i>Galba</i> , <i>Viviparus</i> and <i>Brotia</i>), ostracods, bivalves, charophyte gyrogonites.
A11	Peloidal wackestone-packstone with abundant coated grains and/or calcite rafts	Limestone	Mud-rich carbonate deposits comprising various proportions of crystalline flakes, ostracods and small foraminifera. Facies only found in the St-Chaptes Basin (Unit 3). Decimetre-thick isopachous beds of tight limestones. Subhorizontal, slightly wavy cryptolaminations or calcite rafts (commonly infra-millimetric) are common. May also contain various proportions of subcylindrical calcitic crusts generally composed of one layer of equigranular calcite of similar morphology as the ones of calcitic rafts. Oncoids are also common.			Molluscs (<i>Potamides aporoschema</i>), ostracods and small benthic foraminifera.
A12	Lignite/coal interbedded in marlstone and clays	Lignite to organic-rich marlstone	Decimetre-thick, massive beds, transitional bedding contact, parallel laminations in marlstones.	Aragonitic preserved.	shells are	Plant debris, freshwater gastropods with preserved aragonite (<i>Galba</i> , <i>Viviparus</i> , <i>Brotia</i>), ostracods, charophytes, phytoclasts remains and rare foraminifera.
FA4 - Lacustrine coastal mud-flat						
A13	Argillaceous mudstone-wackestone with mud-cracks, fishes, insects, plant remains, foraminifera and molluscs	Argillaceous limestone	Very thinly laminated (~0.1 mm) argillaceous mudstones (carbonate content: 75 to 90%) commonly affected by desiccation cracks			Well preserved fishes, insects, plant remains, benthic foraminifera and gastropods (<i>Potamides aporoschema</i>)

FA5 - Infralittoral lake

A14	Intraclastic floatstone	Argillaceous limestone	Floatstone with laminated endoclasts (microbial laminae?) embedded in an argillaceous bioclastic wackestone matrix.	-	Characean thalli and gyrogonites; ostracods, benthic foraminifers.
A15	Poorly sorted oncolithic bioclastic grainstone-rudstone alternating with silty marlstone	Limestone to silty marlstone	Oncolitic-molluscan grainstone-rudstone. Decimetre- to metre-thick crudely-laminated beds intercalated within A10 and A17. The base of the oncolithic beds is erosive. Oncoids are generally coarse-grained (typically 1 to 5 mm in diameter) and the nuclei generally consist of mollusc fragments. The cortex is made of continuous and relatively isopachous micrite laminae.	Formation of calcite spars occurs in the intergranular pore space	Mollusc fragments
A16	Silty-argillaceous mudstone-wackestone with scattered bivalves and foraminifera	Argillaceous limestone	Dark, laminated argillaceous limestones (mudstone to wackestone texture) with variable carbonate and quartz silt fraction. Laminations are typically horizontal and parallel but convolute structures may occur.	-	Bivalves (<i>Polymesoda</i>), benthic foraminifers (Textulariids)
FA6 - Profundal Lake					
A17	Platy marlstones with scattered bivalves and foraminifers	Marlstone to calcareous marlstone.	Dark-grey platy marlstones and calcareous marlstones with horizontal, planar laminations.	-	Rare molluscs (<i>Polymesoda</i>), common coaly plant remains
A18	Finely laminated, organic-rich marlstone	Marlstone.	Dark, finely laminated marlstone, with horizontal, planar laminations.	-	Unidentified organic debris
A19	Bioturbated organic-rich argillaceous marlstone with abundant pyrite	Argillaceous marlstone.	Dark, bioturbated marlstone.	Common pyrite	Unidentified organic debris
FA7 - Lacustrine delta					
A20	Quartzose peloidal calcilutite	Quartzose calcilutite	Carbonate-mud-supported sediment containing various proportions of fine-to-coarse grained, subangular to subrounded quartz sand particles and peloids (=quartzose peloidal calcilutite or quartzose-peloidal wackestone).	-	Mainly ostracods, rare benthic foraminifera and mollusc fragments.
A21	Medium-to-coarse grained sandstone to quartzose calcarenite	Sandstone to quartzose calcarenite	1-10 centimetre-thick flat-based beds of medium-to-coarse grained sandstones or quartzose calcarenites interbedded within quartzose calcilutites (A20 lithofacies) or silty argillaceous limestones and marlstones (A16-A17 lithofacies). Allochems are essentially composed of quartz grains (40 to 60%) and calcitic peloids (40 to 60%). Deposits could be cross-bedded with mud draped foresets. Top of the beds often exhibits symmetric ripples in the Saint-Chaptes Basin.	Cements are completely lacking and the cohesion of the rock is mainly due to compaction.	Numerous plant debris
FA8 - Dry mud-flat and shallow saline pan					
A22	Breccia with mixed carbonate and siliceous elements (evaporite collapse breccia)	Brecciated limestone	Intra formational poorly-sorted breccia with mixed large carbonate elements of tightly cemented limestones containing abundant silica pseudomorphs after gypsum or leached gypsum crystals occurs as up to 1-50 metre-thick beds in intervals with common silica. The top of these beds are irregular surfaces that can show polygonal cracks filled with gypsum. The uneven top surface of the breccia beds is draped by stromatolitic laminated limestones (facies A3).	The intergranular space between the elements of the breccia may be partially or entirely filled with calcite spar. Pervasive dissolution is locally evidenced, in peculiar stratigraphic interval, leading to the development of dissolution surfaces	No identified biota

A23	Siliceous beds (pseudomorphs after selenitic gypsum)	Silicified pseudomorphs	Strata of silicified prismatic gypsum occur at the base of unit U1 and U2 above major unconformities in the Issirac Basin. Silica pseudomorphs after gypsum are well developed in the lower part of the carbonate succession. Up to 0.50 metre-thick beds of dominantly vertically aligned, large (up to 0.50 m long and 5 mm wide) elongated, stick-like crystals of gypsum, displaying a lense-shape section, and that have been replaced into silica.	Gypsum prismatic crystals are preserved as microquartz (~10 µm) envelopes whereas the inter- and intracrystalline space is partially to entirely occupied by coarser (≥100 µm) drusy, equigranular quartz infills.	No identified biota
A24	Green gypsiferous silty clays	Silty clays with gypsum crystals	Yellow-green to green nonconsolidated silty smectite-rich clays with scattered gypsum nodules (<4 cm), together with remobilized fibrous gypsum along fractures, quartz grains and glauconite. The green gypsiferous silty clays form an interval of variable thickness (up to 60 m in the southern flank of the Issirac Basin and commonly lacking in the northern flank, that unconformably overly the Cretaceous substratum.		No identified biota
FA9 - Saline lake					
A25	Planar to wavy-laminated mudstone/bindstone with sparse lenticular gypsum	Limestone to dolostone with gypsum (+ anhydrite relicts)	Planar to wavy laminated limestones and dolostone embedding sparse lenticular gypsum crystals, up to 0.3 mm in diameter (Fig 7A to B). They are found as: 1) polycrystalline secondary gypsum or anhydrite pseudomorphs, and 2) dissolution voids partially or entirely filled with calcite cement or bitumen. Gypsum spherulites are also present (Fig. 8F). The coalescence of lenticular gypsum crystal may lead to the formation of nodules (Figs 7A and 8G). Wavy laminations are partly related to displacive growth of gypsum within the sediment (Fig. 7A). However, preferential thickening of laminae at top of small-scale undulations and corrugations suggests a microbial original for such laminae.	(Early?) replacement of gypsum by anhydrite and later, partial transformation of anhydrite into gypsum, dissolution of anhydrite and/or gypsum, sparry calcite cements in molds.	Rare ostracods
A26	Planar to wavy-laminated mudstone/bindstone with vertical, elongated grass-like gypsum crystals	Dolostone and gypsum (+ anhydrite relicts)	Planar to wavy-laminated dolomicrites interbedded with layers of elongated (up to 1cm long), subvertical, prismatic and smaller (<500 µm) lense-shaped gypsum crystals (Fig. 7C). The larger, grass-like elongated crystals exhibit relicts of an anhydrite precursor (Fig. 7E).	(Early?) replacement of gypsum by anhydrite and later, partial transformation of anhydrite into gypsum.	No identified biota
A27	Dolomitic mudstone with large, scattered, prismatic to elongated lenticular gypsum crystals	Dolostone and gypsum (+ anhydrite relicts)	Large (1-10 cm) prismatic to elongated gypsum crystals embedded in a structureless to planar-laminated dolomitic mudstone (Fig. 8D). Laminae are not disturbed around large crystals thus suggesting replacement of micrite into gypsum/anhydrite. Large crystals are dominantly composed of polycrystalline gypsum with rare relicts of anhydrite.	Crystals are commonly leached, filled with bitumen or replaced by dolomicrite.	No identified biota
A28	Irregularly laminated nodular gypsum/anhydrite alternating with laminated dolomicrite	Laminated gypsum (+ anhydrite relicts), dolomicrite laminae, native sulphur	Alternating planar to wavy laminar dolomicrite (1-10 mm thick intervals) and centimetre-thick layers of coalescent gypsum/anhydrite nodules (Figs 8A to C and 8E). Nodules mainly consists of secondary polycrystalline gypsum with rare relicts of anhydrite. Anhydrite/gypsum may be partially replaced by native Sulphur (Fig. 8C).	Partial transformation of anhydrite into gypsum. Partial replacement of anhydrite/gypsum by native sulphur. Fractures are common and are frequently filled with fibrous (satin spar) gypsum.	No identified biota

Table 4. Definition, description and palaeoenvironmental interpretation of the depositional lithofacies from the Priabonian Alès, Saint-Chaptes and Issirac (ASCI) lake system (A1 to A28). Lithofacies codes from Alès Basin (AB1 to AB14) and those used in previous publications (Lettéron et al., 2017, 2018) have also been reported.

Generalized facies classification (ASCI lake system):					Facies classifications			
Facies association classes	Paleo-environments	Facies associations	Facies code	Lithofacies	Alès Basin: this paper	Issirac Basin: Lettéron et al., 2017	Saint-Chaptes Basin: Lettéron et al., 2018	
Carbonate dominated facies associations	Palustrine	FA1	A1	Brecciated-nodular and clotted-peloidal limestones	AB1	F3	P3	
			A2	Thinly-bedded oncolithic-bioclastic grainstone	-	-	P4	
	Shallow lake or littoral	FA2.1	A3	Planar-laminated bindstone	-	F4	SLC8	
			FA2.2	A4	Peloidal packstone-grainstone with abundant molluscs, ostracods and benthic foraminifera	-	F6.3	SLC6
				A5	Ooidal packstone-grainstone	-	F6.1	-
				A6	Molluscan grainstone-rudstone (= coquina)	-	F6.2	-
				A7	Peloidal mudstone-wackestone with molluscs, ostracods and benthic foraminifera	-	F5	SLC2
Mixed carbonate-terrigenous facies associations	Wetlands (ponds, swamps and marshes)	FA3	A8	Silty claystones with sideritic rhizoconcretions	-	-	P2	
			A9	Very fined-grained quartz-rich peloidal packstone-grainstone	-	-	MTC2	
			A10	Fossiliferous marlstone and argillaceous marlstone	AB2	-	MTC1	
			A11	Peloidal wackestone-packstone with abundant coated grains and/or calcite rafts	-	-	SLC4	
			A12	Lignite/coal interbedded in marlstone and clays	AB3	-	P1	
			A13	Argillaceous mudstone-wackestone with mud cracks, fishes, insects, plant remains, benthic foraminifera and molluscs (=Papyraceous argillaceous limestone)	-	-	SLC5	
	Lacustrine coastal mud-flat (eulittoral)	FA4	A14	Intraclastic floatstone	AB4	-	-	
			A15	Poorly-sorted oncolithic bioclastic grainstone-rudstone alternating with silty marlstone	-	-	SLC7	
			A16	Silty-argillaceous mudstone-wackestone with scattered bivalves and foraminifera	AB5	-	-	
			A17	Platy marlstones with scattered bivalves and foraminifers	AB6	-	SLC1	
Profundal lake	FA6.1	A18	Finely laminated, organic-rich marlstone	AB7	-	-		
		FA6.2	A19	Bioturbated organic-rich argillaceous marlstone with abundant pyrite	AB8	-	-	
		A20	Quartzose peloidal calcilutite	AB9	-	-		
Terrigenous-dominated facies associations	Lacustrine delta	FA7	A21	Medium-to-coarse grained sandstone to quartzose calcarenite	AB10	-	MTC3	
			A22	Breccia with mixed carbonate and siliceous elements (evaporite collapse breccia)	-	F1	-	
Evaporite-bearing facies associations	Dry mud-flat and shallow saline pan	FA8	A23	Siliceous beds (pseudomorphs after selenitic gypsum)	-	F2	-	
			A24	Green gypsiferous silty clays	-	F0	-	
			A25	Planar to wavy-laminated mudstone/bindstone with sparse lenticular gypsum	AB11	-	-	
	Saline lake	FA9	A26	Planar to wavy-laminated mudstone/bindstone with vertical, elongated grass-like gypsum crystals	AB12	-	SLC3	
			A27	Dolomitic mudstone with large, scattered, prismatic to elongated lenticular gypsum crystals	AB13	-	-	
			A28	Irregularly laminated nodular gypsum/anhydrite alternating with laminated dolomicrite	AB14	-	-	

*Facies Association 2 – Shallow lake facies association (eulittoral to upper littoral) – Shallow lacustrine carbonates include a variety of depositional lithofacies: planar-laminated bindstone (A3 lithofacies); peloids packstone-grainstone with abundant molluscs, ostracods and/or benthic foraminifera (A4 lithofacies); ooid packstone-grainstone (A5 lithofacies); fragmented mollusc bioclast grainstone-rudstone (A6 lithofacies); and peloidal mudstone-wackestone with molluscs, ostracods and benthic foraminifera (A7 lithofacies). The upper littoral environment (FA2.1) has been distinguished from the strict lower littoral environment (FA2.2) by the common occurrence of planar-laminated bindstone, characean gyrogonites and shallow-water molluscs (see Lettéron *et al.*, 2017; Table 3).*

Mixed carbonate-terrigenous facies associations

*Facies Association 3 – Wetlands facies association (ponds, swamps and marshes) – FA3 facies association includes: silty claystones with sideritic rhizcretions (A8 lithofacies); very fine-grained quartz-rich peloidal packstone-grainstone (A9 lithofacies); marlstone and argillaceous marlstone (A10 lithofacies); peloidal wackestone to packstone with abundant coated grains and/or calcite rafts (A11 lithofacies); and lignite or coal interbedded in marlstones and clays (A12 lithofacies). The high content of sand-sized quartz particles in lithofacies A9, the repeated occurrences of palustrine lithofacies and associated lignites (A12 lithofacies) as well as carbon and oxygen stable isotope signatures, provide evidence of a humid climate (Lettéron *et al.*, 2018). Lignites, charophytes, freshwater gastropods, ostracods, calcite rafts and sideritic rhizcretions are suggestive of swamp or pond palaeoenvironmental conditions. Such interpretations are also supported by the palynological assemblage which is dominated by semi-aquatic fern spores (*Osmundaceae*, *Gleicheniaceae*, *Polypodiaceae*, *Sparganiaceae* and *Schizaeaceae-Lygodium*) (Lettéron *et al.*, 2018). Sideritic beds (A8 lithofacies) (see lithofacies P2 in Lettéron *et al.*, 2018 – Table 3) associated with lignites (A12 lithofacies)*

have been interpreted as back-swamp paludal deposits close to meandering streams in an alluvial floodplain lake with frequent overflows (e.g. Bojanowski *et al.*, 2016). Massive beds of lithofacies A9 associated with lignites may represent shallow deltaic sediments in a lake with positive inflow-evaporation balance (e.g. Gierlowski-Kordesch, 2010).

Facies Association 4 – Lacustrine coastal mud-flat facies association – FA4 facies association is mainly composed of argillaceous mudstone to wackestone with fishes, insects, plant remains, foraminifera and rare shell fragments. Well-preserved in the Saint-Chaptes Basin, it consists of very thinly laminated argillaceous mudstones (ca 0.1 mm) showing a 'paper-like' stratification. Papyraceous argillaceous limestones commonly exhibit desiccation cracks and hence suggest deposition in the shallow lake margin (Lettéron *et al.*, 2018).

Facies Association 5 – Perennial, shallow lake facies association – FA5 lithofacies association includes: intraclastic floatstone (A14 lithofacies) (Fig. 6E and F); poorly-sorted oncolytic-bioclastic grainstone to rudstones alternating with silty marlstone (A15 lithofacies); and silty-argillaceous mudstone-wackestone with bivalves and foraminifera (A16 lithofacies) (Fig. 6G and H). All of these lithofacies are indicative of a perennial, low energy, relatively shallow and well-oxygenated water body.

Facies Association 6 – Perennial, oxygen-poor lake facies association – Laminated, organic-rich, dark grey mudstone and marlstone characterize this facies association. FA6 consists of platy, dark-grey marlstone and calcareous marlstone (A17 lithofacies); azoic, finely laminated, argillaceous mudstone (A18 lithofacies); and organic-rich, argillaceous marlstone with abundant pyrite (A19 lithofacies) (Fig. 6I and J). All of these lithofacies are indicative of a perennial, low energy and poorly-oxygenated water body.

Terrigenous dominated facies associations

Facies Association 7 – Shallow lacustrine delta facies association – FA7 consists of a plurimetre-thick succession of vertically stacked, quartzose calcilutites (A20 lithofacies) (Fig. 5K) and fine to medium-grained sandstones to quartzose calcarenites (A21 lithofacies) (Fig. 5L and M). They are reported exclusively from the Saint-Chaptes (Lettéron *et al.*, 2018) and southern Alès basins (= Célas Sandstone Formation - CSF - Fig. 2). The high-terrigenous content (>40%), the common symmetrical ripples, cross-bedding deposits with mud drape foresets as well as the occurrence of benthic foraminifera and subaqueous molluscs are indicative of shallow lacustrine deltaic environments.

Calcium sulphate-dominated facies

Facies Association 8 – Dry mud-flat and shallow saline pan facies association – The FA8 facies association has been identified in various intervals from the Issirac and Saint-Chaptes basins. It includes: mixed calcium sulphate and carbonate collapse breccia (A22 lithofacies); silica pseudomorphs after gypsum (selenite) (A23 lithofacies); and green gypsiferous silty clays (A24 lithofacies). It should be stated such depositional lithofacies and associated diagenetic features characterize almost solely the margins of the evaporitic area as dry mud-flat or shallow saline pan (Lettéron *et al.*, 2017).

Facies Association 9 – Evaporitic lake facies association – The FA9 facies association includes: planar to wavy-laminated mudstone to bindstone with sparse lenticular gypsum (A25 lithofacies) (Fig. 7A and B); planar to wavy-laminated mudstone to bindstone with vertical, elongated grass-like gypsum crystals (A26 lithofacies) (Fig. 7C to E); dolomitic mudstone with large, scattered, prismatic to elongated lenticular gypsum crystals (A27 lithofacies) (Figs 7F, 7G and 8D); and nodular gypsum/anhydrite alternating with laminated dolomicrite (A28 lithofacies) (Fig. 8A to E). All of these lithofacies are indicative of evaporitic lake environments from marginal (A25–A26) to lake centre (A27–A28) settings.

The chronostratigraphic framework of the Alès, Saint-Chaptes and Issirac lake system

The correlation scheme between Issirac, Saint-Chaptes and Alès basins (Fig. 11) and the chronostratigraphic framework (Fig. 12) of the ASCI Priabonian lacustrine deposits have been established by coupling the present magnetostratigraphic interpretations and the available published mammal (Rémy, 1994, 1999, 2015) and charophyte (Feist-Castel, 1971; Lettéron *et al.*, 2017) biostratigraphic constraints. The locations of charophyte and mammal-based chronostratigraphic constraints are displayed in Figs 2, 10A and 12.

Two major episodes of increased aridity and hydrological isolation of the ASCI lake system were highlighted: (i) during the early mid-Priabonian, the Lower Evaporitic Interval (LEI - Fig. 11) is a thick (ca 100 m) calcium sulphate-rich interval (gypsum and anhydrite) confined to the deeper part of the ASCI lake system (Alès Basin); (ii) during the late Priabonian the ASCI palaeolake system recorded a second thick succession of calcium sulphate in the Alès Basin (Upper Evaporitic Interval, UEI - Fig 12). In areas of shallow-water lacustrine sedimentation, such as interpreted in the Issirac and Saint-Chaptes basins, two maximum aridity events have also been recorded: base of U1 unit and top U1 unconformity / base U2 in Issirac (Lettéron *et al.*, 2017), top U3/ base U4 and top U5/base U6 in Saint-Chaptes (Lettéron *et al.*, 2018). These two Priabonian aridity events (LEI and UEI), recorded in the three sub-basins, are attributable to stages of maximum regression of the lake (exposure surface in Issirac, Saint-Chaptes as well as in Les Fumades area in the Alès Basin) and have been used as key stratigraphic markers for correlations within the ASCI lake system. Additional significant exposure surfaces (surface of maximum regression) have been used as correlatable surfaces across the three sub-basins (Fig. 12).

Among the four proposed magnetostratigraphic interpretations from the Issirac Basin database, hypothesis 1 appears to be the most likely since it does not imply the existence of a long-term hiatus encompassing a normal polarity chron. Additionally, hypotheses 2 and 4 would be

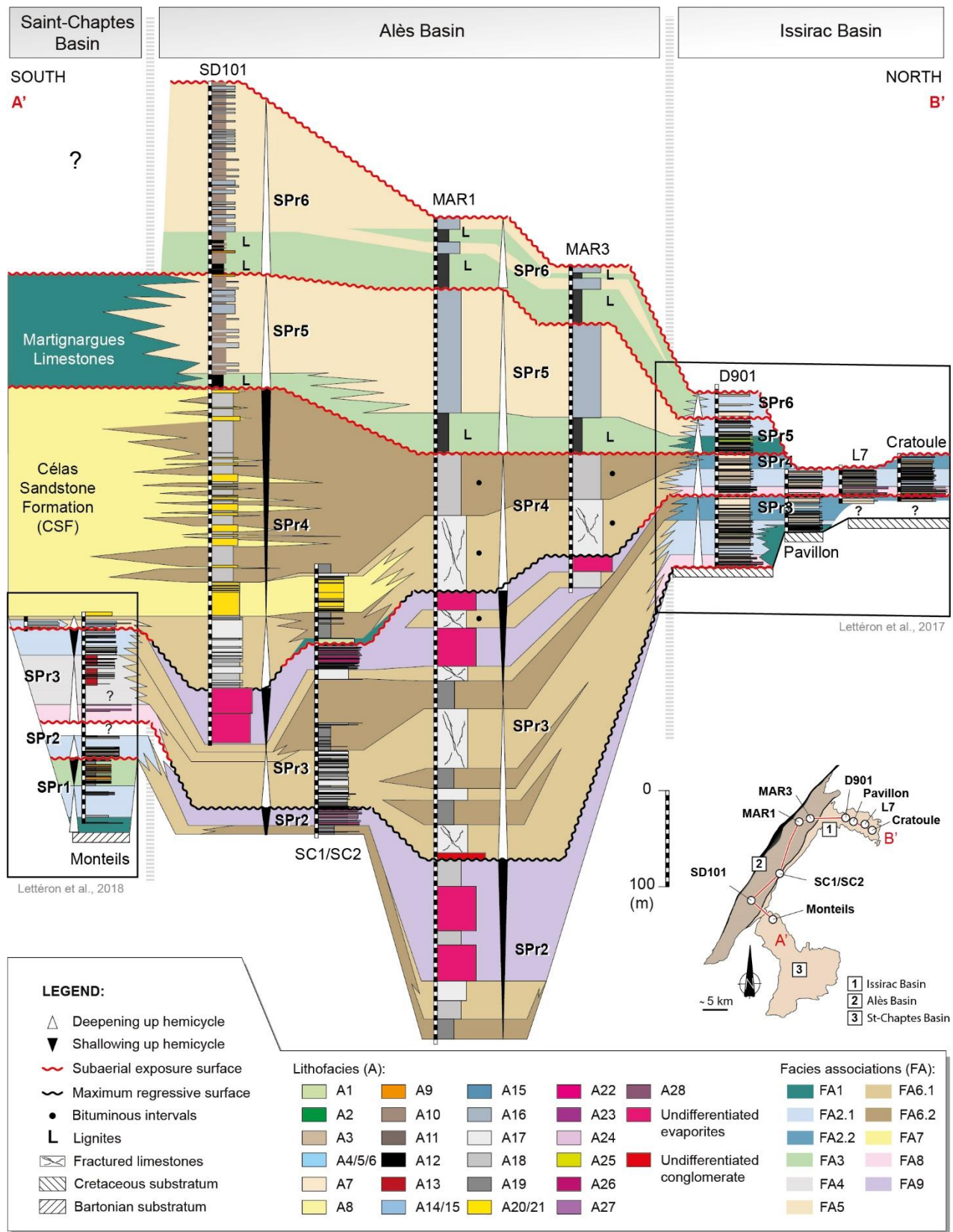


Fig. 11. Correlation panel between wells and outcrops, through the Priabonian deposits of the Alès, Saint-Chaptes and Issirac (ASCI) lake system, along a north-south transect. Well colours refer to ASCI lithofacies classification (cf. Table 3) and background correlations colours refer to facies associations (FA) (cf. Table 4).

inconsistent with the Priabonian age of the UEI yielded by mammal and charophyte biostratigraphy in the Saint-Chaptes and Alès basins. One implication of the magnetostratigraphic analysis coupled with charophyte biostratigraphy is that an early Rupelian age cannot be excluded for the upper part of the carbonate succession in the Issirac Basin (U3 unit).

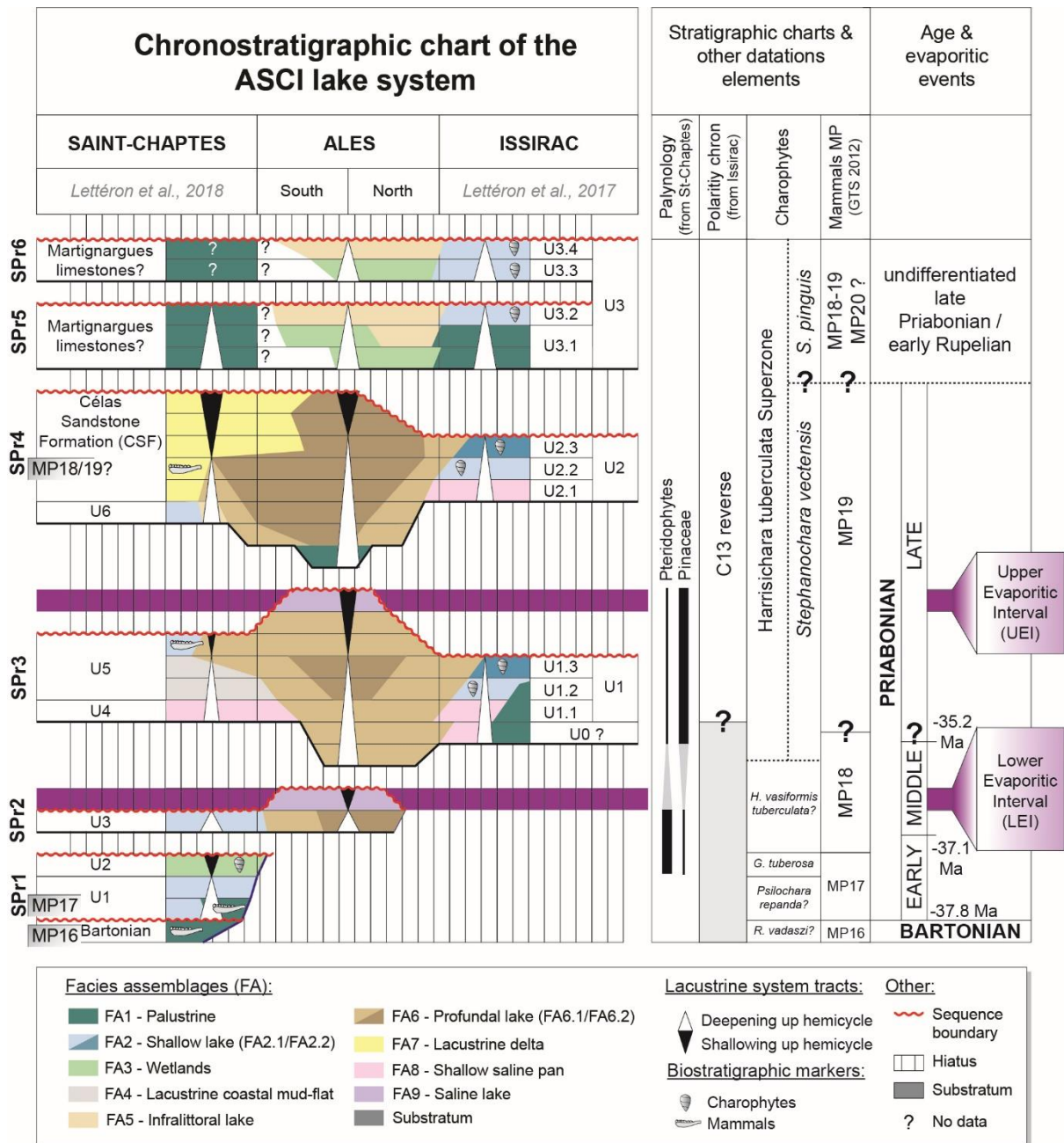


Fig. 12. Chronostratigraphic chart of the Priabonian deposits in the Alès, Saint-Chaptes and Issirac (ASCI) lake. Charophyte biostratigraphy derives from Feist-Castel (1971) and Lettéron et al. (2017, 2018) and mammal biostratigraphy from Rémy (1994, 1999, 2015) and Aguilar et al. (1997). Charophyte reference levels from Riveline et al. (1996).

Definition of depositional sequences in the Priabonian Alès, Saint-Chaptes and Issirac basin lake deposits

The vertical evolution of depositional lithofacies in marginal (Lettéron *et al.*, 2017, 2018) and profundal lake settings as well as the chronostratigraphic correlations between the Alès, Saint-Chaptes and Issirac basins (Fig. 12) allowed subdivision of the ASCI lake succession into six depositional sequences (SPr1 to SPr6) bounded by subaerial exposure surfaces and correlative maximum regression surfaces (Figs 4, 11 and 12). The chronostratigraphic subdivisions adopted within the Bartonian and Priabonian refer to the mammal zonation (late Bartonian = MP16; early Priabonian = MP17; middle Priabonian = MP18; and late Priabonian = MP19) after Vandenberghe *et al.* (2012).

SPr1 sequence (late Bartonian to early Priabonian)

The earliest ASCI lake deposits unconformably overlie the poorly dated early to middle Bartonian? siliciclastics. The age of these deposits range from the late Bartonian (MP16 mammal biozone in Robiac, southern Saint-Chaptes Basin - Rémy, 2015) to early Priabonian (MP17 biozone from: (i) Euzet fossiliferous locality, Saint-Chaptes Basin - Depéret, 1917; Lettéron *et al.*, 2018); and (ii) Souvignargues, Sommières Basin - Stehlin, 1905). In the Saint-Chaptes Basin, the SPr1 transgressive hemicycle (=unit U1 in Lettéron *et al.*, 2018) is characterized by an upward transition from palustrine (FA1) to perennial lacustrine carbonates (FA2). They are overlain by a siliciclastic (FA7) interval ('Serre de Cauvel sandstones' in Alabouvette *et al.* (1983) and 'unit U2' in Lettéron *et al.*, 2017), whose upper part is characterized by the occurrence of lignite horizons with root traces (FA3), thus suggesting a regressive pattern. SPr1 deposits are lacking in the Alès and Issirac basins (Figs 11 and 12).

SPr2 sequence (middle Priabonian)

In the Saint-Chartes Basin, the SPr2 sequence starts with transgressive, brackish-water, lacustrine deposits (FA2) whereas in the Alès Basin (for example, MAR-1 and SC-1 wells) the early SPr2 deposits are profundal lake marlstones (FA6) (Figs 4A, 4D and 11). In the Alès Basin, SPr2 sequence exhibits an upward transition from FA6 marlstones to FA9 calcium sulphates thus suggesting a major lake level drop and lake regression (Figs 4A and 4D). Even though not observed in the field, the Alès Basin SPr2 calcium sulphates likely correlate in the Saint-Chartes Basin with a subaerial exposure surface (top SPr2 = top of U3 in Lettéron *et al.*, 2018) (Figs 11 and 12).

SPr3 sequence (late Priabonian)

In the Alès Basin, SPr2 calcium sulphates are overlain by profundal lake marlstones (FA6) which is consistent with a lake transgression. In the Saint-Chartes and Issirac basins, the SPr3 transgression is inferred from the vertical succession of dry mud-flat and shallow saline pan sulphates (FA8), overlain by shallow lacustrine carbonates (FA2). In such marginal domains, only the transgressive interval of the SPr3 sequence has been recorded (Lettéron *et al.*, 2017, 2018). In the Alès Basin, a subsequent regressive interval is recorded as a thick (up to 100 m) calcium sulphate-rich unit (FA9) that is topped in SC-2 well by a subaerial exposure surface (= top SPr3) (Fig. 4D). Such a major unconformity likely correlates with the top U1 subaerial exposure surface from the Issirac Basin that records a major drop in the ASCI lake level (Lettéron *et al.*, 2017) (Figs 11 and 12). In contrast, in MAR-1 and MAR-101, the top SPr3 sequence is a conformable surface without evidence of subaerial exposure which indicates that even during the maximum of lake regression, a residual lake remained in the north-western part of the Alès Basin.

SPr4 sequence (late Priabonian)

In the Saint-Chaptes Basin, after a shallow lake transgression, the SPr4 sequence corresponds to the development of a prograding, siliciclastic, lacustrine depositional system (Lettéron *et al.*, 2018). In the Alès Basin, palustrine carbonates (FA1) overlying the top SPr3 evaporite unconformity likely represent the lowermost transgressive deposits of the SPr4 ASCI lake system (Fig. 4D). They vertically change into profundal lake marlstones (FA6) thus representing the transgressive hemicycle of the SPr4 sequence (Fig. 4D). The regressive hemicycle is characterized, in the Alès Basin, by an upward transition from FA6 marlstones to wave-rippled, fine to medium-grained sandstones and quartzose calcarenites (FA7), that represent lacustrine shoreface environments (Fig. 4A and D). Such a regressive trend is related to the northward progradation of the Célas sandstone siliciclastic system (e.g. Séranne *et al.*, 2002) (Figs 11 and 12). The Issirac Basin was, at the time of SPr4 sequence development, disconnected from the southern siliciclastic inputs. The SPr4 sequence is characterized, in the Issirac Basin by a vertical transition from dry mud-flat evaporites (FA8) to perennial shallow, saline lake carbonates. Such a transgressive trend is interrupted at the top by a subaerial exposure surface (top SPr4 = top U2 in Lettéron *et al.*, 2017), thus suggesting a significant lake level drop (Figs 11 and 12).

SPr5 and SPr6 sequences (late Priabonian to early Rupelian?)

In the Alès Basin, SPr5 and SPr6 sequences exhibit the same vertical evolution with a basal lignite-bearing freshwater palustrine interval (FA3) containing abundant freshwater molluscs (*Brotia*, *Galba* and *Viviparus*) and characean gyrogonites, overlain by lacustrine carbonates with brackish water biota (FA4 and FA5) thus suggesting a transgressive pattern coupled with an increase in salinity (Fig. 4A). Such sequences are capped by a subaerial exposure surface, without deposition of evaporites. Similar transgressive trends are recorded in the Issirac Basin (Unit U3 in Lettéron *et al.*,

2017) by the upward vertical transition from FA1 freshwater palustrine carbonates to FA2 saline lake deposits (Figs 11 and 12) which suggest that salt water inflow increased during transgression.

DISCUSSION

Lacustrine depositional models

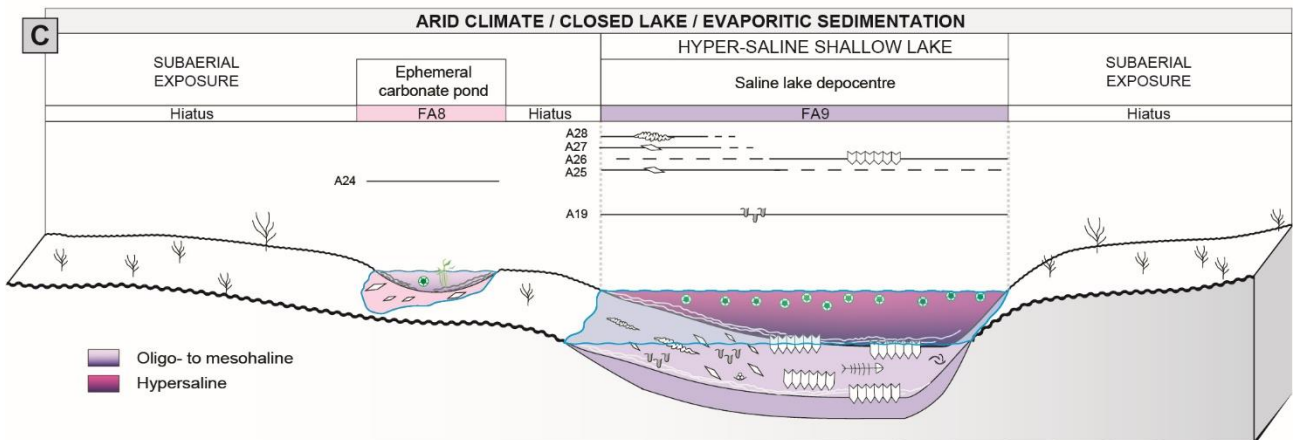
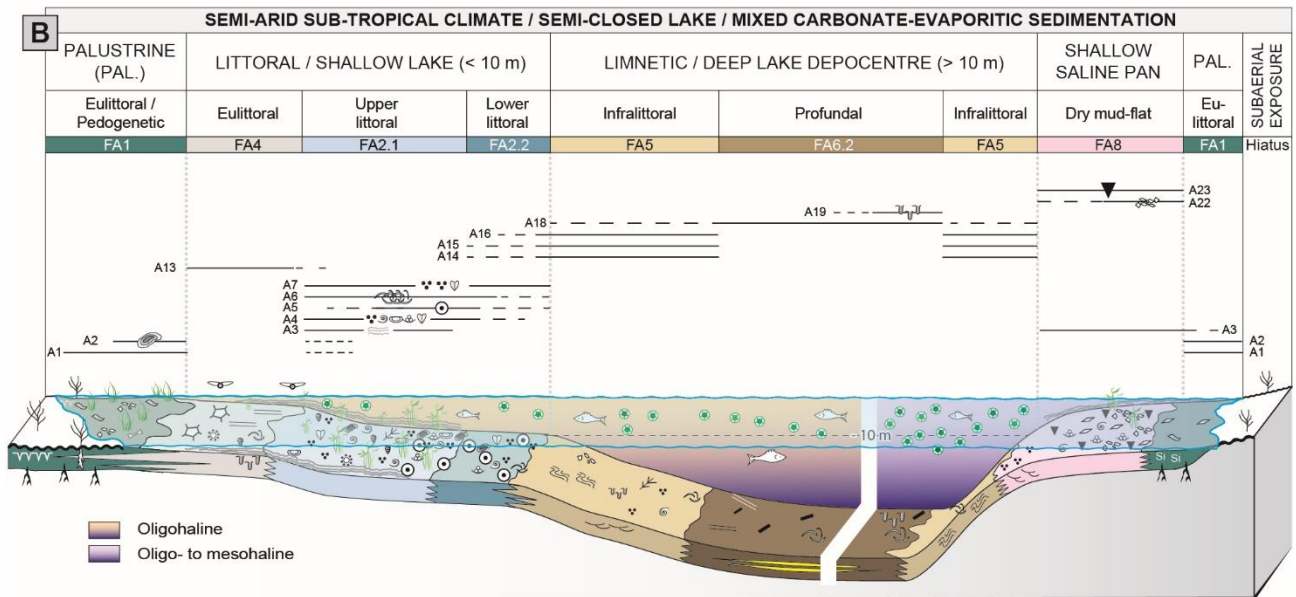
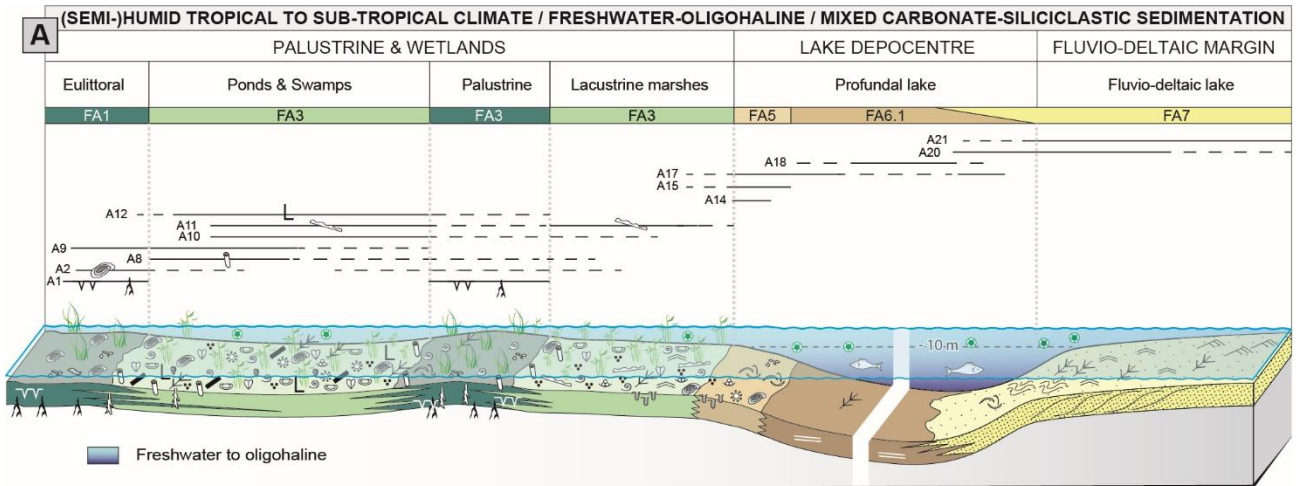
The palaeoenvironmental interpretations of depositional lithofacies, coupled with regional chronostratigraphic correlations allowed us to reconstruct three depositional models of the ASCI lake system (Fig. 13).

Freshwater to oligohaline lake model

The basin-fill deposits from sequences early SPr1, late SPr4, SPr5 and SPr6 allow reconstructing a non-evaporitic, dominantly freshwater to oligohaline lake model (Fig. 13A). The latter is characterized by a dominance of palustrine (FA1) and wetland (FA3) sedimentation in the lake margins with significant development of lignite horizons (A12 lithofacies) and/or by siliciclastic inputs (FA7) supplied into the lake system. In deeper-water setting, sedimentation is dominated by platy marlstones (A17 lithofacies), and claystones to argillaceous marlstones with no preserved benthos (A18 lithofacies).

Lignite horizons are mostly preserved in the Alès Basin depocentre during the early phase of lacustrine transgression (particularly at base SPr5 and SPr6). In the marginal areas (Saint-Chaptes and Issirac), lignite horizons are thinner and rare, likely as a result of lower subsidence rates which favour the development of long-duration exposures that therefore prevent the preservation of organic matter. A principal clastic system installed in the south during SPr4 thus leading to the northward progradation of deltaic sand bodies into the Alès Basin ('Célas Sandstone Formation': FA7 facies association). Riverine freshwater input forced a salinity gradient. Mollusc assemblages and benthic

foraminifera show that waters are fresh or oligohaline at the mouth of the delta system (Saint-Chaptes Basin), and are mostly oligohaline to mesohaline in the northern Alès Basin (Maruejols-1 well: this paper) and in the Issirac Basin (Lettéron *et al.*, 2017). The significant development of palustrine carbonates suggests high frequency rainfall events to carry the carbonate-rich solutions in surface waters or in the groundwater (De Wet *et al.*, 1998). Semi-arid to sub-humid climates with marked seasonality are considered to explain the accumulation and preservation of palustrine carbonate deposits (Platt & Wright, 1991; Sanz *et al.*, 1995; Gierlowski-Kordesch, 1998). In addition, organic-rich palustrine and lake margin carbonates interbedded with coal measures, such as those evidenced in the Alès Basin (A12 lithofacies: Fig. 4), are indicative of sub-humid conditions (Alonso-Zarza & Calvo, 2000). Terrigenous inputs during the deposition of the SPr4, SPr5 and SPr6 sequences, as well as the highlighted desalination compared to underlying sequences, strongly suggest significant riverine water inflow. Finally, the almost lack of evaporite minerals within SPr4, SPr5 and SPr6 sequences is consistent with a positive or moderately negative hydrological balance. These sedimentological results are consistent with palaeoclimatic inversion analyses based on fossil leaf physiognomy which has been performed on palaeobotanical material collected at the base of sequence SPr4 near Célas locality (Tanrattana *et al.*, 2020). Using the CLAMP (Climate Leaf Analysis Multivariate Program) approach, the estimated mean annual precipitation (1464 to 1867 mm) and mean annual temperature (19 to 19.7°C) indicate subtropical humid conditions, whereas estimated precipitation in drier months suggests the existence of a dry season. Finally, the persistence of saline conditions during SPr4 (particularly in the Issirac basin) and the increasing salinity recorded during SPr4 and SPr5 transgressions suggest a connection with a neighboring salt-water reservoir.



- | | | | | | | |
|-------------|----------------------|-----------------------|----------------------|----------------------|-------------------------------------|---------------|
| Vertebrates | Benthic foraminifera | Fenestrae | Lignite | Slumps | Lenticular gypsum | Higher plants |
| Fishes | Bioclasts | Plant debris | Calcite rafts | Wavy ripples | Silica pseudomorphs after gypsum | Macrophytes |
| Insects | Oncolites | Stem/roots concretion | Bioturbation | Current ripples | Vertically oriented gypsum crystals | Phytoplankton |
| Ostracods | Ooids | Roots | Gyrogenites | Trough cross-bedding | Nodular anhydrite | Periphyton |
| Gastropods | Peloids | Organic debris | Charophyte thalli | Desiccation cracks | Shrinkage cracks | Substrate |
| Bivalves | Intraclasts | | Parallel laminations | Si Chert | | |

Fig. 13. Depositional models of the Alès, Saint-Chaptes and Issirac (ASCI) lake system. (A) Humid tropical to sub-tropical climate, mixed carbonate-siliciclastic sedimentation in a freshwater to oligohaline lake system. (B) Semi-arid sub-tropical climate, closed lake, mixed carbonate-evaporitic sedimentation. (C) Arid climate, closed lake, evaporitic sedimentation. The definition of the depositional lithofacies is given in Table 3 and facies associations in Table 4.

Oligohaline to mesohaline closed-lake model

During stages of lake system transgression and highstand from sequence SPr2 (early part), SPr3 and SPr4 (Fig. 13B), widespread shallow lacustrine carbonate sedimentation (FA2) occurred in marginal areas (Saint-Chaptes and Issirac basins) with a significant development of planar-laminated microbial bindstone (A3 lithofacies) and foraminiferal, ostracodal and peloidal mudstone-wackestone (A7 lithofacies). In deep-water settings, density-stratification related to higher salinities favoured the preservation of organic matter below the pycnocline (Sonnenfeld, 1985) thus leading to the deposition of organic-rich marlstones (A19 lithofacies). Dominantly oligohaline to mesohaline conditions prevailed as evidenced by foraminiferal and molluscan assemblages in marginal lake setting (Lettéron *et al.*, 2017, 2018) as well as by the regular occurrence of benthic foraminifera in lake system depocentre lithofacies (this paper, Fig. 4). Calcium sulphates have been shown to mostly form in salt pans or saline mud flats (FA8) during early stages of lake transgressions. These specific evaporite deposits are recorded in the well-extended ASCI lake system margins developed in Saint-Chaptes (Lettéron *et al.*, 2018) and Issirac (Lettéron *et al.*, 2017) basins. The occurrence of such calcium sulphates in marginal settings implies the existence of dry periods and palaeohydrological closures. Palustrine carbonates are common on top of metre-scale shallowing upward parasequences (Lettéron *et al.*, 2017). The dominance of brecciated-nodular fabrics is evidence of short periods of exposure and rewetting along lake shorelines or in wetlands (Alonso-Zarza & Wright, 2010). In addition, the covariance between carbon and oxygen isotope ratios from Issirac (Lettéron *et al.*, 2017) and Saint-Chaptes (Lettéron *et al.*, 2018) basins suggested closed lake conditions. This is consistent with the almost lack of sand and coarser-grained terrigenous sediments within the ASCI lake system during

SPr2 and SPr3 sequence deposition which suggests relatively low riverine water inputs. Finally, palynological data from the Saint-Chaptes Basin (Gruas-Cavagnetto *et al.*, 1972; Alabouvette *et al.*, 1983) suggested that vegetation developed on dry substrates. As a consequence, the proposed depositional model for the ASCI lake system during SPr2 and SPr3 lake transgressions and highstand characterizes a saline closed-lake environment which likely developed under semi-arid to sub-humid climatic setting with marked seasonality.

Hypersaline lake model

Periods of lake regression (late SPr2 and SPr3 sequences) are marked by the formation of a hypersaline lake (Fig. 13C), which is spatially restricted to the ASCI lake system depocentre area (Alès Basin), while the adjacent basins (Issirac and Saint-Chaptes) are permanently subaerially exposed. Evaporitic sedimentation is mostly characterized by thin (centimetre to decimetre-scale) alternations of gypsum/anhydrite laminae and micritic intervals, enriched in clay and organic matter. In the main depocentre, the dominant laminated gypsum (A25 and A26 lithofacies) as well as the lack of subaerial exposure features suggest relatively shallow, perennial saline lake environments. The occurrence of nodular gypsum/anhydrite (A28) lithofacies at top of SPr3 sequence is interpreted as resulting from the diagenetic transformation of laminated gypsum precursor during the complete drying of the ASCI lake system. Such a calcium sulphate-rich facies association (laminated/nodular gypsum) is similar to that evidenced in Priabonian saline lakes from the Rhône Valley (Triat & Truc, 1974) and the Ebro Basin ('Association B' in Ortí *et al.*, 2007). Such a lake model prone to calcium sulphate precipitation suggests evaporitic settings where a forced regression of the lacustrine base level is driven by negative inflow-evaporation balance.

Diachronous formation of evaporites between lake depocentre and lake margins

Based on the correlation of depositional sequences between the Alès Basin and adjacent areas (Saint-Chaptes and Issirac basins), diachronous formation of calcium sulphate-rich units between the lake depocentre and the margins has been evidenced (Fig. 14). The ASCI chronostratigraphic framework (present study) highlights the non-unique response of such lacustrine system regarding timing and nature of evaporite deposits. In the Alès Basin, calcium sulphate-rich intervals occur in the late SPr2 and SPr3, below major subaerial exposure surfaces. In contrast, evaporitic units have been evidenced above the major regional exposure events, at the base of SPr3 and SPr4 sequences from the Issirac and Saint-Chaptes basins. Hence, centre-lake calcium sulphates are interpreted to be formed during major lacustrine base level fall which resulted from an increased negative inflow–evaporation balance. In contrast, in marginal areas, calcium sulphates mainly form during early lake transgression, in saline mud flats or isolated salt pans (Fig. 14). Transgressive evaporite sedimentation on adjacent and marginal basins implies that the inflow–evaporation balance is still negative while the lake volume expands. Such a condition may be favoured as a result of a marked seasonality which can lead to a partial or complete disconnection of marginal water bodies during dry periods. Evaporitic deposits from Issirac and Saint-Chaptes basins (FA8) have been shown: (i) to have formed in shallow ephemeral ponds; (ii) to be interbedded with shallow lacustrine planar-laminated bindstones (A3 lithofacies); and (iii) to be affected by repeated subaerial exposure surfaces (Lettéron *et al.*, 2017, 2018), thus suggesting the occurrence of various stages of evaporation and reflooding. The deposition of evaporites in such settings may be favoured by the saline nature of water during reflooding. Since no evaporitic rocks are present in the local catchment area of these basins, a return to saline conditions during transgression may be interpreted as resulting from surface and/or groundwater connections with regional saline lakes (for example, Rhône valley rift basins: e.g. Rouchy, 1997).

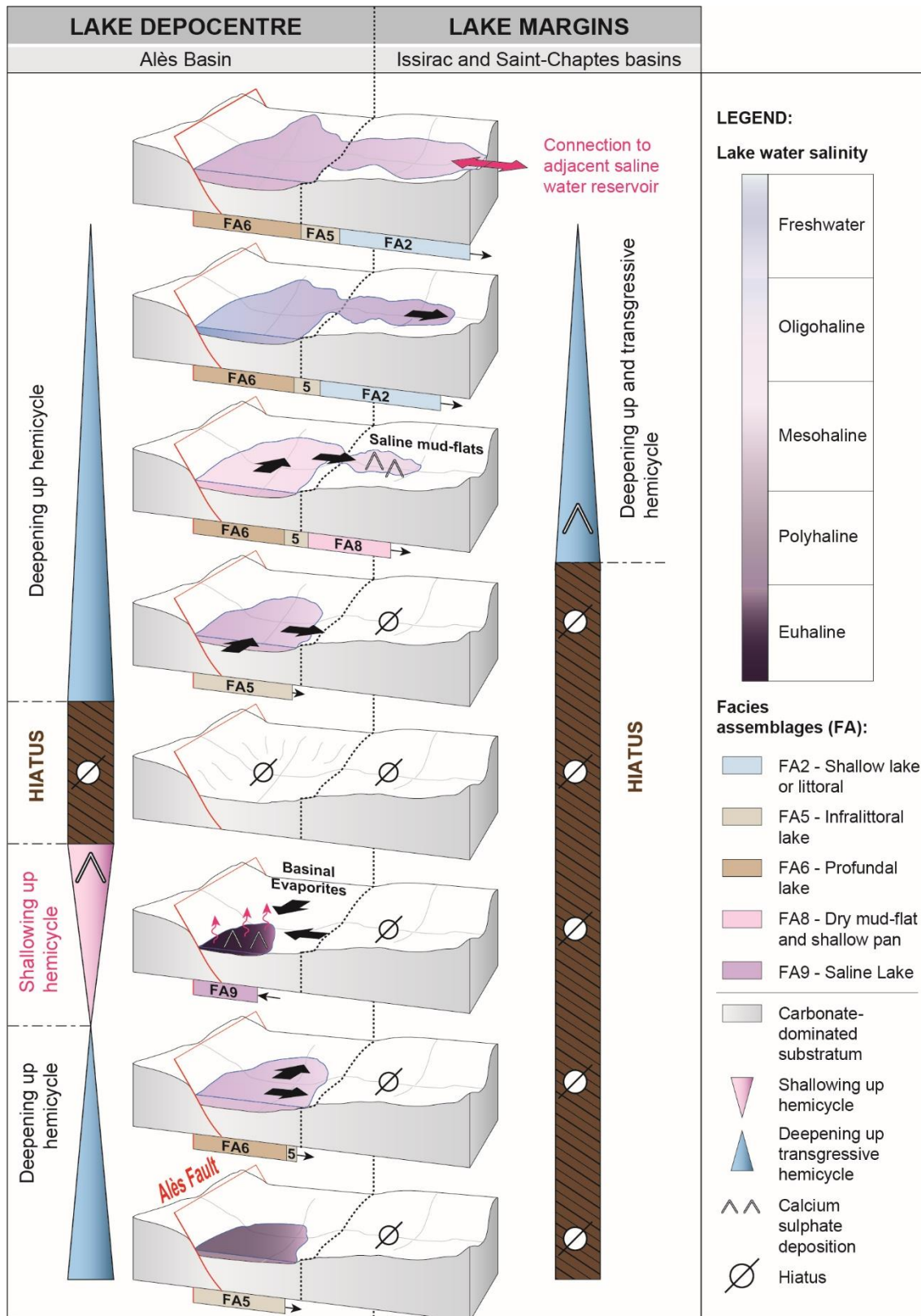


Fig. 14. Stratigraphic correlation scheme showing the distribution in time and space of the lacustrine facies associations from the depocentre to the lake margins. This figure also highlights the basin scale diachronism of salt deposits as well as the timing and lateral extension of sedimentary hiatus (erosion and non-deposition).

Saline lake models in rift basins: a key for continental palaeoclimate reconstructions?

Calcium sulphates are known historically to be sensitive indicators of local and global climatic conditions (e.g. Eugster, 1982). The present work has established that sedimentary archives from the ASCI saline lake system have recorded an evolution through times of depositional facies and palaeoenvironments in response to changing degrees of hydrological closure. A long-term cyclicity in palaeohydrological closure of the ASCI lake has been evidenced from repeated transitions from a freshwater to oligohaline lake to a hypersaline lake model. Two major stages of lake spreading (early to middle Priabonian: late SP_{r1} to early SP_{r2} and late Priabonian: SP_{r4} to SP_{r6}) and two stages of significant lake contraction (middle to late Priabonian: late SP_{r2} and SP_{r3}) have been recorded from the ASCI deposits. However, although the present work has shown that saline lake depositional models from the ASCI depositional system are largely controlled by the degree of palaeohydrological closure, comparisons with adjacent basins are needed to separate local changes due to hydrology or tectonics from regional climatic trends. Indeed, the floral turnover from humid tropical to dryer subtropical taxa evidenced in the ASCI lake system (Gruas-Cavagnetto, 1972; Alabouvette *et al.*, 1983) has also been recorded in the same time interval as in the ASCI lake (SP_{r2}: middle Priabonian), within the 'Green Lymnaea Marls II' formation in the Upper Rhine Graben (URG) (Schuler, 1990) and within the 'Lucina Marls' formation in the Paris Basin (Châteauneuf, 1980). Finally, a return to more humid conditions has been recorded, similarly to the Alès Basin in the late Priabonian from the Upper Rhine Basin (Schuler, 1990). Such a palaeoclimatic trilogy (humid periods during the early and late Priabonian separated by a dry stage during the middle Priabonian) has been also evidenced from mineralogical assemblages and $\delta^{15}\text{N}_{\text{org}}$ in the Rennes Basin (Tramoy *et al.*, 2016). As a result, changing saline lake depositional models and associated palaeohydrological balance in the ASCI lake system are consistent palaeoclimate changes recorded at continental scale during Priabonian stage.

Although aridity cycles appear to be correlated regionally and beyond, the role of local tectonics on the hydrology of the ASCI lake system must also be considered. The hydrological isolation of a lake can be favoured by the development of a barrier of tectonic origin which disconnects it from possible outlets of neighboring lakes. In the case of the ASCI lake system, the roll-over anticline developing east of the Alès Basin (Sanchis & Seranne, 2000) may have physically disconnected the ASCI lake from the coeval Vistrenque and Mormoiron lake basins (Fig. 1). The modification of the reliefs in the footwall may also have modified the drainage area downstream of the lake basin. Thus in an arid climate context, the formation of tectonic reliefs can promote rapid drying up of the lake. In addition, the existence of tectonic barriers will promote the infill and transgression of the lake during a phase of less aridity (e.g. Stephenson, 1986), and the lacustrine areas will develop in topographic lows such as the subsiding areas. The northward lake transgression, from the Saint-Chaptes Basin to the Salindres and Murujols area during the early to middle Priabonian likely result from the development of the Alès hemi-graben (Sanchis & Seranne, 2000). Finally, the development of transgressive hemicycles capped by an emersion surface without evaporite deposition (SPr5 and SPr6) can be interpreted as resulting from a phase of lake infill followed by its emptying due to the formation of an outlet allowing water to escape to another basin. Such an outlet may have formed due to the erosion of a topographic barrier under humid climatic conditions (Garcia-Castellanos, 2006) or may result from fast and tectonically-controlled changes in regional topography (Arzhannikov *et al.*, 2018). Additionally, the connection with neighbouring saline lakes, as evidenced by salinity trends during transgressions, may be both favoured by lake spreading as a result of a positive hydrological balance and by the tectonically induced formation of topographic thresholds. The ASCI case study is a conspicuous example of the difficulty of deconvolving climatic and tectonic parameters controlling the development of sequences in syn-tectonic lake basins.

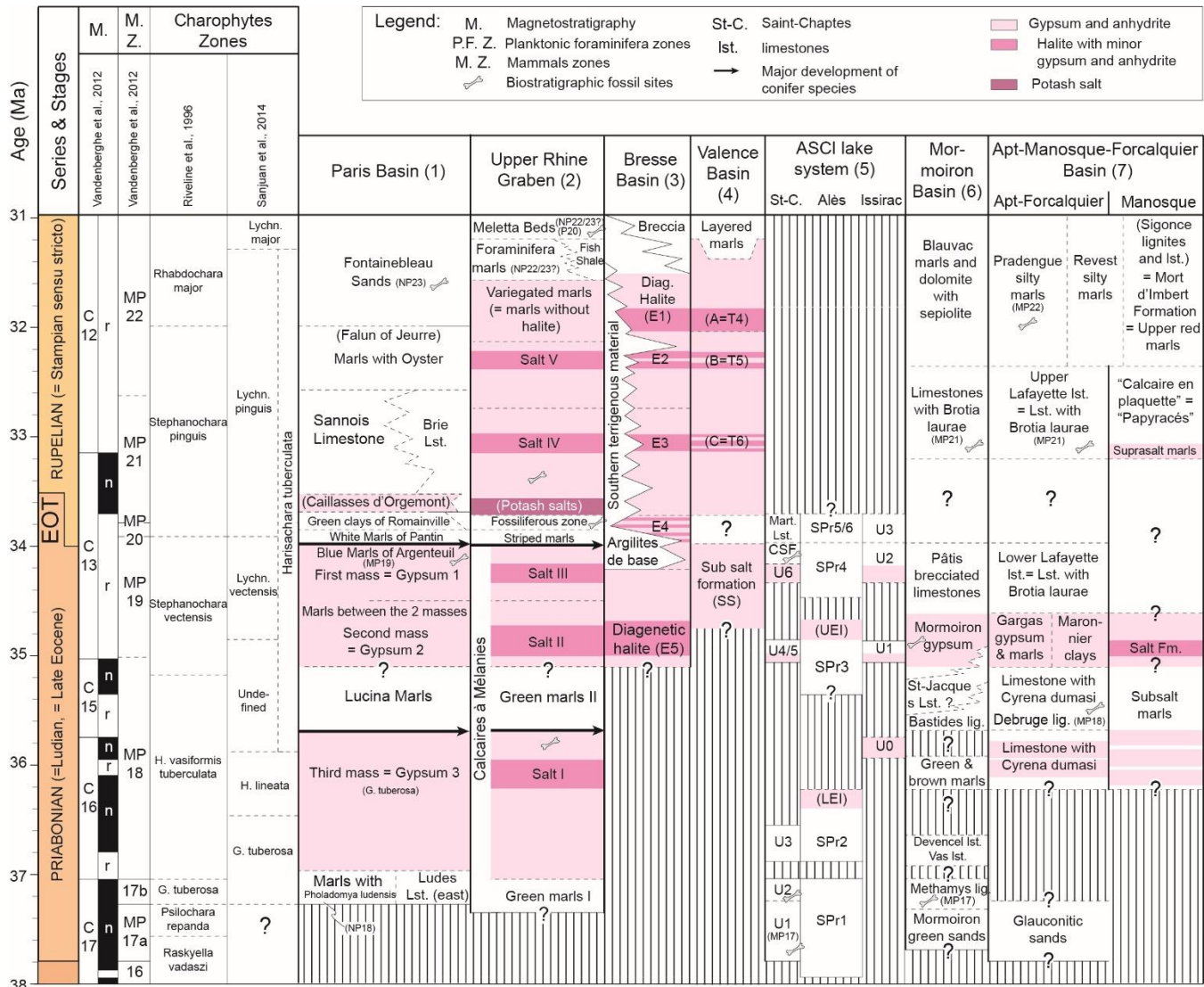


Fig. 15. Stratigraphic correlation chart synthesizing the stratigraphic distribution of Priabonian-Rupelian formations and associated evaporite-rich intervals of the: Paris Basin (1), Upper Rhine Graben (2), Bresse Basin (3), Valence Basin (4), Alès, Saint-Chaptes and Issirac (ASCI) lake system (5), Mormoiron Basin (5), Apt-Manosque-Forcalquier Basin (7) and Rennes Basin (8). The chronostratigraphic framework of: (1) the Paris Basin has been compiled from Lettéron et al. (2018) and references therein; – (2) the Upper Rhine Graben from Lettéron et al. (2018) and references therein; – (3) Bresse Basin from Lienhardt (1974); Gudefin (1977); Dumas (1987); Schuler (1990); Fontes et al. (1996); Dromart & Dumas (1997); – (4) Valence Basin from Lettéron et al. (2018) and references therein; – (5) ASCI lake system from Lettéron et al., (2018 and references therein) and this study; – (6) Mormoiron Basin and (7) Apt-Manosque-Forcalquier Basin from from Lettéron et al. (2018) and references therein. Additional abbreviations: C - polarity chron, CSF - Célas Sandstone Formation, EOT - Eocene-Oligocene Transition, Lst. - limestone, MP - Palaeogene mammalian reference level, n - normal polarity, r - reverse polarity.

More broadly, the concepts of climate control on the development of lacustrine depositional sequences could have important applications in the interpretation of vertical facies variations in different syn-rift or post-rift lake systems with variable salinity, and with different degrees of connection

with neighbouring lakes: for example, early Cretaceous syn-rift lakes from the Sergipe-Alagoas basin, Brazil (Favoreto *et al.*, 2021), Aptian post-rift lake from the Tucano Basin, Brazil (Varejão *et al.*, 2019), Plio-Pleistocene from the East African Rift (Bergner *et al.*, 2009; Nutz *et al.*, 2017), early Cretaceous lakes from the Jiuquan rift basin, China (Zhang *et al.*, 2018), Priabonian and Oligocene rift basins from France (Vistrenque Basin - Benedicto *et al.*, 1996; Valence Basin - Dromart & Dumas, 1997; Bresse and URG - Busson *et al.*, 1992).

Implications for the palaeoclimatic record of Priabonian carbonates and evaporites from Western Europe

The vertical changes in depositional features, sequence stratigraphic patterns, palaeofloristic assemblages and geochemical signatures of the Palaeogene lacustrine carbonate succession from the Alès, Saint-Chaptes and Issirac basins provide new constraints into the nature and timing of the palaeoclimatic changes in south-east France prior to the major Eocene-Oligocene boundary climate event.

In the ASCI lake system, an early phase of aridification has been evidenced in the early Priabonian (MP17: Euzet horizons) deposits (Lettéron *et al.*, 2018). Palynological syntheses (Alabouvette *et al.*, 1983; Lettéron *et al.*, 2018) reveal a major turnover in the floral assemblages during the deposition of the late SPr1 sequence (MP17) from the Saint-Chaptes Basin. Vegetation species of the Saint-Chaptes Basin during late SPr1 and early SPr2 sequence deposition suggests a humid tropical to subtropical climate. A major arid episode (LEI - Fig. 12) is recorded at the end of the SPr2 sequence (middle Priabonian, MP18) in the Alès Basin by the deposition of a thick (ca 100 m) succession of calcium sulphates (gypsum and anhydrite). According to the correlation scheme proposed by Lettéron *et al.* (2018) and references therein, this calcium sulphate-rich interval would be time-equivalent with the 'Salt I' from the Upper Rhine Graben and with the 'Third Gypsum Mass' from

the Paris Basin, thus suggesting that an arid episode occurred at the western European scale during the middle Priabonian. A dry subtropical to Mediterranean climate is inferred from palynological assemblages during the early SPr3 sequence in the Saint-Chaptes Basin (Alabouvette *et al.*, 1983; Lettéron *et al.*, 2018). The stable isotope signatures from the Issirac (Lettéron *et al.*, 2017) and Saint-Chaptes basins (Lettéron *et al.*, 2018) suggest short-term (seasonal?) changes in inflow-evaporation balance within the lake. A second episode of major aridity is recorded in the late SPr3 sequence, at the base of the late Priabonian succession (MP19), by the deposition of the UEI in the Alès Basin. The age of the UEI supports a correlation with the Mormoiron gypsum, the halite deposits from the Manosque Basin, the E5 halite from the Bresse Basin, the 'Second Gypsum Mass' from the Paris Basin and the 'Salt II' interval from the URG (supported by palynological studies; e.g. Châteauneuf, 1980; Schuler, 1990). Such a correlation would support a second major arid climate event in Western Europe during the late Priabonian (MP19).

During the late Priabonian, a drastic change in hydrological balance is recorded in the ASCI lake. Indeed, significant surface water inflows are inferred from: (i) the development of a siliciclastic lacustrine fluvio-deltaic system (Célas Sandstone Formation: SPr4 sequence) in the Sommières, Saint-Chaptes and Alès basins; and (ii) the freshening of the Alès lake during SPr4 deposition as suggesting by the dominance of freshwater molluscs and the scarcity of benthic foraminifera while oligo-mesohaline conditions prevail in the Issirac Basin. Such a palaeohydrological change is consistent with the return to more humid conditions during the late Priabonian in Western Europe as evidenced in the Rennes Basin (Tramoy *et al.*, 2016) and in the Upper Rhine Basin (Schuler, 1990). Persistence of relatively humid conditions are also supported in SPr5 and SPr6 deposits by the development of palustrine carbonates and the deposition of lignites. In Fig. 15, the major aridity events, recorded by thick Priabonian evaporite sedimentation are summarized for Western Europe. The continental-scale correlatability of such evaporitic intervals is indicative of the sensitivity of lacustrine sedimentation to

stages of aridification. Lacustrine systems with mixed carbonate, siliciclastic and evaporite sedimentation extensively developed in Western Europe during the Priabonian in rift basins (e.g. Triat & Truc, 1974; Schuler, 1990; Lesueur, 1991; Blanc-Valleron & Schuler, 1997; Dromart & Dumas, 1997) and the ASCI lake system may therefore be regarded as a relevant example for depositional models, stratigraphic architecture and depositional sequence development of syn-rift Palaeogene lake basins from Western Europe.

CONCLUSIONS

A multi-proxy approach, integrating sedimentological, palaeontological and magnetostratigraphic analyses on both well cores and outcrops provided insights on the stratigraphic architecture of the Alès-Saint-Chaptes-Issirac (ASCI) lake system in a chronostratigraphic framework. Sedimentary archives from the ASCI saline lake system have recorded changes in depositional profiles during the early stage of the Eocene-Oligocene Transition, in response to climate, which modified the palaeohydrology, and thus lacustrine interconnectivity:

- 1) The freshwater to oligohaline open-lake model (earliest middle Priabonian and late Priabonian-earliest Rupelian?) is characterized by significant terrigenous supplies into the basin, the accumulation and preservation of coal beds in palustrine and marginal lake settings, and by the extreme scarcity of evaporite deposits.
- 2) An oligohaline to mesohaline closed-lake model (middle Priabonian) is characterized by significant development of marginal lacustrine carbonates dominated by microbialites (planar stromatolites) and by the deposition of organic-rich marls in profundal lake environments. Gypsum deposition occurs in lake margins, within saline mud flats and salt pans.

- 3) A hypersaline lake model (middle-late Priabonian), restricted to the lake basin depocentre area (central Alès Basin) whose sedimentation is dominated by laminar gypsum and nodular gypsum/anhydrite. Such a model characterized a residual, hypersaline, shallow lacustrine / salt pan environment during phases of extreme hydrological closure and lake forced regression.

The succession through time of these three types of depositional models revealed the existence of two major stages of lake spreading (earliest middle Priabonian: late SP_{r1} to early SP_{r2} and late Priabonian: SP_{r4} to SP_{r6}) and two stages of significant lake closure (middle to late Priabonian: late SP_{r2} and SP_{r3}) which led to the deposition of two main calcium sulphate-rich intervals in the Alès Basin depocentre. Variations in lake closure during the Priabonian have been shown to result in a diachronous formation of evaporite deposits: thick (up to 100 m) laminated/nodular gypsum intervals in the Alès Basin depocentre during phases of major hydrological closure and lake regression, and thin (ca 10 m) units of laminated/selenitic gypsum in adjacent basins (Saint-Chaptes and Issirac) during lake transgressions. Beyond conventional lacustrine stratigraphic models (e.g. Bohacs *et al.*, 2000) driven by inflow/evaporation balance, this study highlighted the complex interplay of climate changes and salinity of water inputs from neighbouring water masses.

The chronostratigraphic correspondence between the palaeohydrological cycles from the ASCI lake system and the major climatic events identified at regional and continental scale for the Priabonian period strongly support a climatic control on the nature of lacustrine depositional models and consequently on the depositional architecture of Palaeogene, syn-rift, saline lake basins from Western Europe.

ACKNOWLEDGMENTS

This work is part of the PhD thesis of the first author (AL) and was funded by IFP Energies Nouvelles (grant number XRP09 001). The authors thank P. Marques (STC core library), P. Vigouroux (BRGM) and G. Coste (Allègres-les-Fumades mayor) and city hall staff for the access to cores. We are grateful to A. Nimy (Aix-Marseille University) for palaeomagnetic data acquisition. Many thanks to J.-A. Rémy for fruitful discussions on the regional geology. Chief Editor Prof. Giovanna Della Porta, Associate Editor Dr. Ola Kwiecien, Dr. Luis Valero, Dr Alexis Nutz and two other anonymous reviewers are gratefully acknowledged for their reviews and valuable comments made on earlier versions of this paper. Thanks to Elaine Richardson for the precious comments.

SUPPLEMENTARY DATA

Supplementary Material - Table. Palaeomagnetic results with statistics (Kirschvink, 1980) and interpretations. Note that due to the large overprints, 23 samples are characterized by great circles, the inclination and declination corresponding to the pole of the calculated planes. Dir Kir - determination of the stable magnetization using least squares method (Kirschvink, 1980); GC Kir - determination for the great circle, i.e. the plane fitting the distribution of magnetizations using least squares method (Kirschvink, 1980); N - number of demagnetization steps used in statistical determinations; D - declination of the stable magnetization or of the pole of the great circle; I - declination of the stable magnetization or of the pole of the great circle; MAD - maximum angular deviation; Interm. - Intermediate polarity; R - Reverse polarity; N - Normal polarity.

DATA AVAILABILITY STATEMENT

The data that support the findings of this study are available from the corresponding author upon reasonable request.

REFERENCES

- Aguilar, J.-P., Legendre, S. and Michaux, J.** (1997) Actes du Congrès Biochrom'97 Montpellier, 14-17 Avril. Biochronologie mammalienne du Cénozoïque en Europe et domaines reliés. *Mémoires et Travaux de l'Institut de Montpellier de l'Ecole Pratique des Hautes Etudes*, **21**, 1-181.
- Alabouvette, B., Chedhomme, J., Frédet, J.M. and Lartaud, V.** (1983) Inventaire des ressources nationales de charbon : lignites du fossé d'Alès-Barjac. *Bur. Rech. Géol. Min. Mém.*, **83**, Orléans, 63 pp.
- Alonso-Zarza, A.M. and Calvo, J.P.** (2000) Palustrine sedimentation in an episodically subsiding basin: the Miocene of the northern Teruel Graben (Spain). *Palaeogeogr. Palaeoclimatol. Palaeoecol.*, **160**, 12-21.
- Alonso-Zarza, A.M. and Wright, V.P.** (2010) Palustrine carbonates. In: *Carbonates in continental settings: facies, environments and processes*, (Eds A.M. Alonso-Zarza and L.H. Tanner), 1st edition, pp. 103-131. Elsevier, Amsterdam.
- Andeweg, B.** (2002) Cenozoic tectonic evolution of the Iberian Peninsula: effects and causes of changing stress fields. PhD thesis, Vrije Universiteit, Amsterdam, Netherlands, 178 pp.
- Arenas, C. and Pardo, G.** (1999) Latest Oligocene-Late Miocene lacustrine systems of the north-central part of the Ebro Basin (Spain): sedimentary facies model and palaeogeographic synthesis. *Palaeogeogr. Palaeoclimatol. Palaeoecol.*, **151**, 127-148.
- Armenteros, I., Daley, B. and García, E.** (1997) Lacustrine and palustrine facies in the Bembridge Limestone (late Eocene, Hampshire Basin) of the Isle of Wight, southern England. *Palaeogeogr. Palaeoclimatol. Palaeoecol.*, **128**, 111-132.
- Arzhannikov, S.G., Ivanov, A.V., Arzhannikova, A.V., Demonterova, E.I., Jansen, J.D.**
- Preusser, F., Kamenetsky, V.S. and Kamenetsky, M.B.** (2018) Catastrophic events in the Quaternary outflow history of Lake Baikal. *Earth-Science Reviews*, **177**, 76-113.
- Benedicto, A., Labaume, P., Séguret, M. and Séranne, M.** (1996) Low angle crustal ramp and basin geometry in the Gulf of Lion passive margin: Oligocene-Aquitainian Vistrenque graben, SE France. *Tectonics*, **15**, 1192-1212.
- Benedicto-Esteban, A.** (1996) Modèles tectono-sédimentaires de bassins en extension et style structural de la marge passive du golfe du lion (partie nord), sud-est France. PhD thesis, Université de Montpellier, France, 255 pp.
- Bergner, A.G.N, Strecker, M.R., Trauth, M.H., Deino, A., Gasse, F., Blisniuk, P. and Dühnforth, M.** (2009) Tectonic and climatic control on evolution of rift lakes in the Central Kenya Rift, East Africa. *Quat. Sci. Rev.*, **28**, 2804-2816.
- Blanc-Valleron M.-M. and Schuler M.** (1997) The Salt Basins of Alsace (Southern Rhine Graben). In: *Sedimentary Deposition in Rift and Foreland Basins in France and Spain (Paleogene and Lower Neogene)* (Eds G. Busson and B.C. Schreiber). Columbia Univ. Press, New York, 95-135.

- Bohacs, K.M., Carroll, A.R., Neal, J.E. and Mankiewicz, P.J. (2000)** Lake-basin type, source potential, and hydrocarbon character: an integrated sequence-stratigraphic-geochemical framework. In: *Lake basins through space and time* (Eds E.H. Gierlowski-Kordesch and K.R. Kelts), *AAPG Studies in Geology*, **46**, 3-34.
- Bojanowski, M., Jaroszewicz, E., Kořir, A., Łoziński, M., Marynowski, L., Wysocka, A. and Derkowski, A. (2016)** Root-related rhodochrosite and concretionary siderite formation in oxygen-deficient conditions induced by a ground-water table rise. *Sedimentology*, **63**, 523-551.
- Busson, G., Blanc-Valleron, M.-M., Cornée, A., Curial, A., Dromart, G., Dumas, D., Moretto, R., Rouchy, J.-M. and Schreiber, C.B. (1992)** Bassins paléogènes salifères de l'Est de la France (Valence, Bresse et Haute Alsace). *Géologie de la France*, **1**, 15-64.
- Cavelier, C. (1965)** Le Sannoisien de Sannois (Seine-et-Oise) dans le cadre du Bassin de Paris et signification stratotypique. *Bull. Soc. Géol. Fr.*, **7** (28), 228-238.
- Chedhomme, J. and Gaudant, J. (1984)** Sur une nouvelle espèce du genre *Palaeoatherina* Gaudant (Poissons Teleosteens, Atherinomorpha) Découverte dans l'Eocène supérieur continental des environs d'Ornagnac-L'Aven (Ardèche). *Géol. Méditerran.*, **11**, 303-319.
- Corzo, A., Luzon, A., Mayayo, M.J., van Bergeijk, S.A., Mata, P. and García de Lomas, J. (2005)** Carbonate Mineralogy Along a Biogeochemical Gradient in Recent Lacustrine Sediments of Gallocanta Lake (Spain). *Geomicrobiology Journal*, **22**, 6, 283-298.
- Costa, E., Garcés, M., Sáez, A., Cabrera, L. and López-Blanco, M., (2011)** The age of the "Grande Coupure" mammal turnover: New constraints from the Eocene-Oligocene record of the Eastern Ebro Basin (NE Spain). *Palaeogeogr. Palaeoclimatol. Palaeoecol.* **301**, 97-107
- Daley, B. (1972)** Macroinvertebrate assemblages from the Bembridge marls (Oligocene) of the Isle of Wight, England, and their environmental significance. *Palaeogeogr. Palaeoclimatol. Palaeoecol.*, **11**, 11-32.
- De Wet, C., Yocum, D.A. and Mora, C. (1998)** Carbonate lakes in closed basins: sensitive indicators of climate and tectonics: an example from the Gettysburg Basin (Triassic), Pennsylvania, USA. In: *Relative Role of Eustasy, Climate and Tectonism in Continental Rocks*. (Eds K.W. Shanley and P.J. McCabe), *SEPM Spec. Publ.*, **59**, 191-209.
- Depéret, C. (1917)** Monographie de la faune de mammifères fossiles du Ludien inférieur d'Euzet-les-Bains (Gard), *Annales de l'Université de Lyon*, Lyon, 364 pp.
- Dromart, G. and Dumas, D. (1997)** The salt basin of Valence (France). In: *Sedimentary deposition in rift and foreland basins in France and Spain (Paleogene and lower Neogene)*. (Eds G. Busson, and B.C., Schreiber), pp. 195-300. Columbia University Press, New York.
- Dumas, E. (1987)** La sédimentation détritique dans le fossé salifère paléogène de Valence (Sud-Est de la France). *Géologie Alpine, Mémoire Hors Série*, **13**, 403-407.
- Ellis, G.S., Katz, B.J., Scholz, C. A. and Swart, P.K. (2015)** Organic sedimentation in modern lacustrine systems: A case study from Lake Malawi, East Africa. In: *Paying Attention to*

Mudrocks: Priceless! (Eds D. Larsen, S.O. Egenhoff and N.S., Fishman), *Geol. Soc. of America Spec. Paper*, 515, 19-47.

Elmore, R.D., Muxworthy, A.R. and **Aldana, M.** (2012) Remagnetization and chemical alteration of sedimentary rocks. *Geol. Soc. London Spec. Publ.*, **371**, 1-21.

Embry, A. and **Johannessen, E.** (1992) T-R sequence stratigraphy, facies analysis and reservoir distribution in the uppermost Triassic-Lower Jurassic succession, western Sverdrup Basin, Arctic Canada. In: *Arctic geology and petroleum potential* (Eds T.O. Vorren, E. Bergsager, O.A., Dahl-Stamnes, B. Johansen, E. Lie and T.B., Lund) pp. 121-146. Netherlands, Nor. Pet. Soc. Spec. Publ., 2.

Eugster, H.P. (1982) Chapter 10: Climate Significance of Lake and Evaporite Deposits. In: *Climate in Earth History: Studies in Geophysics* (Ed. National Research Council, 1982), pp. 105-111. The National Academy Press, Washington.

Favoreto, J., Valle, B., Borghi, L., Führ Dal'Bó, P., Mendes, M., Arena, M., Santos, J., Santos, H., Ribeiro, C. and **Coelho, P.** (2021) Depositional controls on lacustrine coquinas from an early cretaceous rift lake: Morro do Chaves Formation, Northeast Brazil. *Mar. Pet. Geol.*, **124**, 104852.

Feist-Castel, M. (1971) Sur les charophytes fossiles du bassin Tertiaire d'Alès (Gard). *Geobios*, **4**, 157-172.

Fontes, J.-C., Gaudant, J., Mélières, F., Filly, A. and **Schlund, J.-M.** (1996) Origine continentale des évaporites paléogènes du fossé de Valence (Drôme): données minéralogiques, isotopiques et paléoécologiques. *Bull. Soc. Géol. Fr.*, **167**, 475-481.

Frédet J.-M. (1987) Tectonique et sédimentation en domaine continental: évolution du bassin paléogène d'Alès (GARD). PhD Thesis, Université Claude Bernard, Lyon I, France, 244 pp.

Freytet, P. (1973) Petrography and paleo-environment of continental carbonate deposits with particular reference to the upper cretaceous and lower Eocene of Languedoc (Southern France). *Sed. Geol.*, **10**, 25-60.

Garcia-Castellanos, D. (2006) Long-term evolution of tectonic lakes: Climatic controls on the development of internally drained basins. In: *Tectonics, Climate, and Landscape Evolution* (Eds S.D. Willett, N. Hovius, M.T. Brandon and D.M. Fisher) *Geological Society of America Special Paper* **398**, Penrose Conference Series, pp. 283-294.

Gierlowski-Kordesch, E. and **Rust, B.R.** (1994) The Jurassic East Berlin Formation, Hartford Basin, Newark Supergroup (Connecticut and Massachusetts): A Saline Lake-Playa-Alluvial Plain System. In: *Sedimentology and Geochemistry of Modern and Ancient Saline Lakes*. (Eds R.W. Renaut and W.M. Last). *SEPM Spec. Publ.*, **50**, 249-265.

Gierlowski-Kordesch, E.H. (1998) Carbonate deposition in an ephemeral siliciclastic alluvial system: Jurassic Shuttle Meadow Formation, Newark Supergroup, Hartford Basin, USA. *Palaeogeogr. Palaeoclimatol. Palaeoecol.*, **140**, 161-184.

Gierlowski-Kordesch, E.H. (2010) Lacustrine Carbonates. In: *Carbonates in continental settings. Facies, environments and processes*. (Eds A.M. Alonso-Zarza and L.H. Tanner), *Developments in Sedimentology*, **61**, 1-101.

Gudfin H. (1977) Recherches sur la géologie profonde - fosse de Valence (Drôme). Bureau de Recherches Géologiques et Minières (BRGM), Orléans, 58 pp.

Harris, P.M., Ellis J. and Purkis, S.J. (2012) Assessing the extent of carbonate deposition in early rift settings. *AAPG Bulletin*, **97**, 27-60.

Hussain, M. and Warren, J.K. (1989) Nodular and enterolithic gypsum: the "sabkha-tization" of Salt Flat playa, west Texas. *Sed. Geol.*, **64**, 13-24.

Kirschvink, J.L. (1980) The least-squares line and plane and the analysis of palaeomagnetic data. *Geophysical Journal of the Royal Astronomical Society*, **62**: 699-718.

Lettéron, A, Fournier, F., Hamon, Y., Villier, L., Margerel, J.-P., Bouche, A., Feist, M. and Joseph, P. (2017) Multi-proxy paleoenvironmental reconstruction of saline lake carbonates: Paleoclimatic and paleogeographic implications (Priabonian-Rupelian, Issirac Basin, SE France). *Sed. Geol.*, **358**, 97-120.

Lettéron, A., Hamon, Y., Fournier, F., Séranne, M., Pellenard, P. and Joseph, P. (2018) Reconstruction of a saline, lacustrine carbonate system (Priabonian, St-Chaptes Basin, SE France): depositional models, paleogeographic and paleoclimatic implications. *Sed. Geol.*, **367**, 20-47.

Lienhardt M.-J. (1974) Synthèse géologique du Bassin de Valence. Document du Bureau de Recherches Géologiques et Minières (BRGM), 74SGN397JAL, 92 pp.

Liu, Z., Pagani, M., Zinniker, D., DeConto, R.M., Huber, M., Brinkhuis, H., Shah, S.R., Leckie, R.M. and Pearson, A. (2009) Global

cooling during the Eocene Oligocene Transition. *Science*, **323**, 1187-1190.

Lobza, V. and Schieber, J. (1999) Biogenic sedimentary structures produced by worms in soupy, soft muds: observations from the Chattanooga Shale (Upper Devonian) and experiments. *J. Sed. Res.*, **69**, 1041-1049.

Loucks, R.G. and Longman, M.W. (1982) Lower Cretaceous Ferry Lake anhydrite, Fairway Field, East Texas: product of shallow-subtidal deposition. In: *Depositional and Diagenetic Spectra of Evaporites*. (Eds C.R. Handford, R.G. Loucks and G.R. Davies), *Soc. Econ. Paleontol. Mineral.*, **3**, 130-173.

Moretto, R. (1988) Observations on the incorporation of trace elements in halite of Oligocene salt beds, Bourg-en-Bresse Basin, France. *Geochem. Cosmoch. Acta*, **52**, 2809-2814.

Newell, A.J. (2018) Rifts, rivers and climate recovery: a new model for the Triassic of England. *Proceedings of the Geologists' Association*, **129**, 352-371.

Nutz, A., Schuster, M., Boës, X. and Rubino, J.-L. (2017) Orbitally-driven evolution of Lake Turkana (Turkana Depression, Kenya, EARS) between 1.95 and 1.72 Ma: A sequence stratigraphy perspective. *Journal of African Earth Sciences*, **125**, 230-243.

Nutz, A., Kwiecien, O., Breitenbach, S.F.M., Cai, Y., Della Porta, G., Danisch, J., Kabiri, L. and Bodin, S. (2019) Fluvio-lacustrine sedimentation in the Agadir-Tissint Feija (Anti-Atlas, Morocco): A promising palaeoclimate archive for the last glacial cycle in northwest Africa. *The Depositional Record*, **5**, 362-387.

- Ogg, J.G.** (2012) Geomagnetic Polarity Time Scale. In: *The Geologic Time Scale 2012*. (Eds F.M. Gradstein, J.G. Ogg, M.D. Schmitz and G.M. Ogg), pp. 85-113. Elsevier, Amsterdam.
- Ortí, F.** (1997) Evaporite sedimentation in the South Pyrenean foredeeps and the Ebro basin during the Tertiary: a general view. In: *Sedimentary Deposition in Rift and Foreland Basins in France and Spain* (Eds G. Busson and B.C. Schreiber), pp. 319-334. Columbia University Press, New York.
- Ortí, F., Pueyo, J.J. and Truc, G.** (1984) Las salinas marítimas de Santa Pola (Alicante, España). Breve introducción al estudio de un medio natural controlado de sedimentación evaporítica somera. *Rev. Inv. Geol.*, **38/39**, 9-29.
- Ortí, F. and Salvany, J.P.** (1997) Continental evaporitic sedimentation in the Ebro basin during the Miocene. In: *Sedimentary Deposition in Rift and Foreland Basins in France and Spain* (Eds G. Busson and B.C. Schreiber), pp. 420-429. Columbia University Press, New York.
- Ortí, F., Rosell, L., Inglès, M. and Playà, E.** (2007) Depositional models of lacustrine evaporites in the SE margin of the Ebro Basin (Paleogene, NE Spain). *Geol. Acta*, **5**, 19-34.
- Platt, N.H. and Wright, V.P.** (1991) Lacustrine carbonates: facies models, facies distribution and hydrocarbon aspects. In: *Lacustrine Facies Analysis* (Eds P. Anadón, L. Cabrera, and K. Kelts), *Int. Assoc. Sedimentol. Spec. Publ.*, **13**, 57-74.
- Pound, M.J. and Salzmann, U.** (2017) Heterogeneity in global vegetation and terrestrial climate change during the late Eocene to early Oligocene transition. *Scientific Reports*, **7**, 1-12.
- Raiswell, R., Buckler, F., Berner, R. and Anderson, T.** (1988) Degree of pyritization of iron as a paleoenvironmental indicator of bottom water oxygenation. *J. Sed. Petrol.*, **58**, 812-819.
- Rémy, J.-A.** (1994) Une faunule de vertébrés sous la base des Grès de Célas (Eocène sup.) à Saint-Dézéry (Gard). *Palaeovertebrata*, **23**, 211-216.
- Rémy, J.-A.** (1999) Deux nouveaux gisements de Vertébrés fossiles dans la formation de Célas (Éocène supérieur du Gard). *Bull. Soc. Etud. Sci. Nat. Nîmes Gard*, **62**, 16-22.
- Rémy, J.-A.** (2015) Les Périssodactyles (Mammalia) du gisement Bartonien supérieur de Robiac (Éocène moyen du Gard, Sud de la France). *Palaeovertebrata*, **39**, 1-98.
- Riveline, J., Berger, J.-P., Feist, M., Martin-closas, C., Schudack, M. and Soulié-Märsche, I.** (1996) European Mesozoic-Cenozoic charophyte biozonation. *Bull. Soc. Geol. France*, **167**, 453-468.
- Rohais, S., Hamon, Y., Deschamps, R., Beaumont, V., Gasparrini, M., Pillot, D. and Romero-Sarmiento, M.-F.** (2019) Patterns of organic carbon enrichment in a lacustrine system across the K-T boundary: Insight from a multi-proxy analysis of the Yacoraite Formation, Salta rift basin, Argentina. *Int. J. Coal Geol.*, **210**, 103208.
- Rouchy, J.-M.** (1997) Paleogene Continental Rift System of Western Europe: Locations of Basins, Paleogeographic and Structural Framework, and the Distribution of Evaporites. In: *Sedimentary Deposition in Rift and Foreland*

Basins in France and Spain (Eds. G. Busson, and B.C., Schreiber), pp. 45-94. Columbia University Press, New York.

Roure, F., Colletta B., Brun, J.-P., Giot, D. and Steinberg, M. (1992) Structure profonde et problèmes de diagénèse dans le bassin du SE. Internal report, Institut Français du Pétrole, IFP, Division Géologie et Géochimie, France, 39446, 75 pp.

Salvany, J.P., Muñoz, A. and Pérez, A. (1994) Nonmarine evaporitic sedimentation and associated diagenetic processes of the southern margin of the Ebro basin (Lower Miocene), Spain. *J. Sed. Res.*, **64**, 190-203.

Samanta, P., Mukhopadhyay, S. and Eriksson, P. (2016) Forced regressive wedge in the Mesoproterozoic Koldaha Shale, Vindhyan basin, Son Valley, Central India. *J. Mar. Petrol. Geol.*, **71**, 329-343.

Sanchis, E. (2000) Méthodologie d'Imagerie 3D des bassins, des exemples dans le Bassin du Sud-Est. Unpublished Report. Technical report, Université de Montpellier and Bureau de Recherches Géologiques et Minières, Orléans, 70 pp.

Sanchis, E. and Séranne, M. (2000) Structural style and tectonic evolution of a polyphase extensional basin of the Gulf of Lion passive margin: the Tertiary Alès basin, southern France. *Tectonophysics*, **322**, 219-242.

Schuler, M. (1990) Environnements et paléoclimats paléogènes. Palynologie et biostratigraphie de l'Eocène et de l'Oligocène inférieur dans les fossés rhénan, rhodanien et de Hesse. Document du Bureau de Recherches Géologiques et Minières (BRGM), **190**, 503 pp.

Séranne M, Couëffé R, Husson E, Baral C, Villard J. (2021) The transition from Pyrenean shortening to Gulf of Lion rifting in Languedoc (South France) –A tectonic-sedimentation analysis. *BSGF - Earth Sciences Bulletin*, **192**: 27.

Sanjuan, J., Martin-Closas, C., Costa, E., Barbera, X. and Garcés, M. (2014) Calibration of Eocene-Oligocene charophyte biozones in the Eastern Ebro Basin (Catalonia, Spain). *Stratigraphy*, **11**, 61-81

Sanz, M.E., Alonso-Zarza, A.M. and Calvo, J.P. (1995) Carbonate pond deposits related to semi-arid alluvial systems: examples from the Tertiary Madrid Basin, Spain. *Sedimentology*, **42**, 437-452.

Séranne, M., Benedicto, A., Labaum, P., Truffert, C. and Pascal, G. (1995) Structural style and evolution of the Gulf of Lion Oligo-Miocene rifting: role of the Pyrenean orogeny. *Mar. Petrol. Geol.*, **12**, 809-820.

Séranne, M., Camus, H., Lucazeau, F., Barbarand, J. and Quinif, Y. (2002) Surrection et érosion polyphasées de la bordure cévenole. Un exemple de morphogénèse lente. *Bull. Soc. Géol. Fr.*, **173**, 97-112.

Shearman, D. (1966) Origin of evaporites by diagenesis. *Trans. Inst. Min. Metall.*, **75**, B208-B215.

Shearman, D. (1983) Syndepositional and late diagenetic alteration of primary gypsum to anhydrite. In: *Sixth International Symposium on Salt* (Eds B.C. Schreiber and H.L. Harner), pp. 41-50. Northern Ohio Geological Society, Cleveland, Ohio.

Sonnenfeld, P. (1985) Evaporite as oil and gas source rocks. *J. Petrol. Geol.*, **8**, 253-271.

- Soták, J.** (2010) Paleoenvironmental changes across the Eocene-Oligocene boundary: insights from the Central-Carpathian Paleogene Basin. *Geol. Carpath.*, **61**, 393-418.
- Stehlin, H.G.** (1905) Die Säugetiere des schweizerischen Eocaens. Critisher Catalog der Materialien. *Abh. Senckenb. Naturforsch. Ges.*, **32**, 447-595.
- Stephenson, A.E.** (1986) Lake Bungunnia; a Plio-Pleistocene megalake in southern Australia. *Palaeogeogr. Palaeoclimatol. Palaeoecol.*, **57**, 137-156
- Taberner, C., Cendon, D.I., Pueyo, J.J. and Ayora, C.** (2000) The use of environmental markers to distinguish marine vs. continental deposition and to quantify the significance of recycling in evaporite basins. *Sed. Geol.*, **137**, 213-240.
- Talbot, M. R.** (1988) The origin of lacustrine source rocks - Evidence from the lakes of tropical Africa. In: *Lacustrine petroleum source rocks* (Eds A.J. Fleet, K. Kelt and M.R. Talbot), *Geological Society Special Publication*, **40**, pp. 29-43.
- Tanrattana, M., Boura, A., Jacques, F., Villier, L., Fournier, F., Enguehard, A., Cardonnet, S., Volland, G., Garcia, A., Chaouch, S. and De Franceschi, D.** (2020) Climatic evolution in Western Europe during the Cenozoic: insights from historical collections using leaf physiognomy. *Geodiversitas*, **42**, 151-174.
- Tramoy, R., Salpin, M., Schnyder, J., Person, A., Sebilo, M., Yans, J., Vaury, V., Fozzani, J. and Bauer, H.** (2016) Stepwise palaeoclimate change across the Eocene-Oligocene transition recorded in continental NW Europe by mineralogical assemblages and $\delta^{15}\text{N}_{\text{org}}$ (Rennes Basin, France). *Terra Nova*, **28**, 3, 212-220.
- Triat, J.M. and Truc, G.** (1974) Evaporites paléogènes du domaine rhodanien. *Rev. Géogr. Phys. Géol. Dynam.*, **16**, 235-262.
- Truc, G.** (1978) Lacustrine sedimentation in an evaporitic environment: the Ludian (Palaeogene) of the Mormoiron basin, southeastern France. *Int. Assoc. Sedimentol. Spec. Publ.*, **2**, 189-203.
- Vandenberghe, N., Hilgen, F.J. and Speijer, R.J.** (2012) The Paleogene period. In: *The Geologic Time Scale 2012*. (Eds F.M. Gradstein, J.G. Ogg, M.D. Schmitz and G.M. Ogg), pp. 855-921. Elsevier, Amsterdam.
- Varejão, F.G., Warren, L.V., Freitas, B.T., Neumann, V.H. and Assine, M.L.** (2019) Saline lake development in the Aptian post-rift phase of the Tucano Basin: Tectonic and paleogeographic implications. *Journal of South American Earth Sciences*, **92**, 282-297.
- Vogel, M.K., Des Marais, D.J., Parenteau, M.N., Jahnke, L.L., Turk, K.A and Kubo, M.D.Y.** (2010) Biological influences on modern sulfates: Textures and composition of gypsum deposits from Guerrero Negro, Baja California Sur, Mexico. *Sedimentary Geology*, **223**, 265-280.
- Wright, P.V.** (2012) Lacustrine carbonates in rift settings: the interaction of volcanic and microbial processes on carbonate deposition. In: *Advances in Carbonate Exploration and Reservoir Analysis* (Eds J. Garland, J.E. Neilson, S.E. Laubach, and K.J. Whidden), Geological Society, London, Special Publications, **370**, pp. 39-47.

Zachos, J.C., Pagani, M., Sloan, L., Thomas, E. and Billups, K (2001) Trends, rhythms, and aberrations in global climate 65 Ma to present. *Science*, **292** (5517), 686-693.

Zhang, C., Muirhead, J.D., Wang, H.W., Chen, S., Liao, Y., Lu, Z. and Wei, J. (2018) Lacustrine fan delta deposition alongside intrabasinal structural highs in rift basins: an example from the Early Cretaceous Jiuquan

Basin, Northwestern China. *International Journal of Earth Sciences*, **107**, 1835-1858.

Zhang, C., Scholz, C.A. and Harris, A.D. (2020) Sedimentary fills and sensitivity analysis of deep lacustrine facies in multi-segment rift basins: Insights from 3D forward modeling. *Sedimentary Geology*, **408**, 105753.